Summer 2021

The Effects of Heterogeneities and Syn-deformational Partial Melting on Rock Strength Evolution and Melt Migration

Nicole Wagner
niw6@uakron.edu

`

The Effects of Heterogeneities and Syn-deformational Partial Melting on Rock Strength Evolution and Melt Migration

Nicole Wagner

Honors Thesis Project

Advisor: Dr. Caleb W. Holyoke III

Readers: Dr. John Peck and Dr. Molly Witter

April 30, 2021

1. Abstract

In nature, the segregation of granitic melts at the source may be controlled by fabric and compositional heterogeneities in the source rock, such as foliation and lineation. To investigate the influence of foliation/lineation orientation and composition on rock strength and melt interconnectivity, I performed a series of experiments on cores of a fine-grained gneiss (Gneiss Minuti) and a fine-grained muscovite-bearing quartzite (Moine Thrust quartzite). These rocks were cored at six primary orientations parallel, 45 degrees, and perpendicular to the foliation and lineation and were deformed at a constant temperature of 900°C, pressure of ~2 GPa, and strain rate of ~10^{-6}/s using the D-DIA apparatus at Beamline 6-BMB at the Advanced Photon Source at Argonne National Laboratory.

Strengths of the Gneiss Minuti cores varied from 1.02 to 1.17 GPa, and strengths of the Moine Thrust quartzite ranged from 1.28 to 1.61 GPa. The strength anisotropy of the cores relative to the core with the foliation oriented 45 degrees to the compression direction varied from 0.87 to 1.99 in the Gneiss Minuti cores and ranged from 0.59 to 2.13 in the Moine Thrust quartzite cores. Melt was present in all cores, and concentrations varied from 1 to 4 vol% for the Gneiss Minuti and from 0.6 to 1.2 vol% for the Moine Thrust quartzite. The Gneiss Minuti and Moine Thrust quartzite cores had similar melt topology in all foliation orientations with small melt channels/pockets parallel to the compression direction, and the only significant melt interconnectivity was observed in the Gneiss Minuti foliation/lineation parallel to the compression direction sample, which also had the largest melt fraction (3.74 vol%). These results indicate that when above a low melt content (~1 to 2 vol%), the presence of melt has a greater effect than the orientation of foliation and lineation on the strength of foliated rocks and melt migration.

2. Introduction

Earthquakes that occur in the brittle upper crust are linked to the middle and lower crust by the transferring of stresses to the lower crust after slip events. Following this transfer of stresses, the rheology of the middle to lower crust can affect aftershock intensity (Bürgmann and Dresen, 2008). To explore this concept, experimental studies are performed in the laboratory to simulate naturally occurring processes that cannot be observed evolving on human timescales. Models such as Bürgmann and Dresen (2008) incorporate experimentally derived rheologies of

isotropic monophase rocks for the middle to lower crust. However, the middle to lower crust is usually composed of rocks with heterogeneities such as foliations and lineations.

Heterogeneities in crustal rocks, such as foliation (planar rock features) and lineation (linear rock features), are known to influence the strength of the crust depending on their orientation within the source rock causing strength anisotropy in both brittle and ductile conditions (Gottschalk et al., 1990; Braccia and Holyoke, 2019). In foliated rocks that undergo brittle deformation, the strength is usually the greatest when the foliation is perpendicular to the compression and the least when the foliation is at 45 degrees to the compression (Gottschalk et al., 1990). These orientations correspond to placing the foliation at orientations that minimize and maximize the shear stress on the foliation, respectively. Comparatively, foliation/lineation orientation under ductile (crystal plastic) conditions, simulating deformation in the middle to lower crust, also appears to influence the strength of rocks. Braccia and Holyoke (2019) performed experiments on a quartzite (87% quartz and 13% muscovite) at conditions with no melt present and where the dominant deformation mechanism is dislocation creep (T = 800°C and $P_{confining}$ = 1.5 GPa). They found that foliation, and more so lineation orientation, creates strength anisotropy. Dislocation creep is a common deformation mechanism in the mid to lower crust that involves the propagation of linear defects along specific crystallographic planes and axes, and the viscous anisotropy described above is a result of this mechanism's sensitivity to the orientation of crystal planes and axes relative to the compression direction. This viscous anisotropy under crystal plastic conditions is also seen in other Earth materials, such as olivine aggregates, where strength differences are generated from the formation of crystallographic preferred orientations (Hansen et al., 2012). These prior studies indicate that the strength in both the upper and lower crust will be anisotropic, but all of these experiments were performed in the absence of syntectonic metamorphic reactions.

Syntectonic metamorphic reactions, including partial melting, have a significant weakening effect on the strength of rocks by disrupting the framework that supports the applied tectonic loads (Dell 'Angelo and Tullis, 1988; Holyoke and Rushmer, 2002; Brown, 2007). Dell 'Angelo and Tullis (1988) observed that partial melting can decrease the strength of granitic aggregates (natural and synthetic aplites) by changing the dominant deformation mechanism from dislocation creep to diffusion creep (diffusion of atoms along grain boundaries from high stress sites to low stress sites), or cataclasis (fracturing of grains throughout the aggregate). In

addition, the composition of rocks and/or melting reactions can affect the operating deformation mechanisms. Composition controls melting reactions, melt viscosity, and how readily melt channels and pockets can interconnect and segregate from source rock (Rushmer, 2001). Composition can also influence deformation through the volume changes that occur in the transition of solid material to melt plus solids (Rushmer, 2001; Holyoke and Rushmer, 2002). Field based observations indicate that melt interconnection and segregation might also be affected by rock fabric heterogeneities, such as foliation and lineation (Brown, 2007). In this study, I will investigate the influence of foliation/lineation orientation and partial melting on rock strength evolution as well as examine the effects of foliation/lineation and source rock composition on melt migration.

3. Procedure

3.1 Starting Materials

In order to investigate the influence of foliation/lineation orientation and partial melting on rock strength and melt segregation, I cored and deformed two naturally occurring foliated rocks: the Gneiss Minuti collected in Nivetta, Italy (Zurbriggen et al., 1998) and the Moine Thrust quartzite collected from the sample location AS-3 of the Allt nan Sleach section of the Assynt exposure of the Moine Thrust in Eriboll, Scotland (Law et al., 1986). The Gneiss Minuti is a natural, fine-grained gneiss consisting of 43% quartz, 40% plagioclase, 16% biotite, and 1% other phases with an average grain size of 30 ± 16 microns (Figure 1). The foliation in the Gneiss Minuti is defined by aligned biotite grains isolated in a framework of quartz and plagioclase. The Moine Thrust quartzite, is a natural fine-grained quartzite composed of quartz and muscovite with an average grain size of 33 ± 14 microns (Braccia and Holyoke, 2019) (Figure 2). The muscovite in the quartzite defines the foliation and is generally, isolated in a quartz framework. These rocks were selected because they should undergo dehydration melting reactions and form granitic melts at the conditions of this study (Rushmer, 2001).

3.2 Experimental Techniques

Experiments for this study were performed by deforming stacked cores of the Gneiss Minuti or the Moine Thrust quartzite using the D-DIA apparatus at Beamline 6-BMB at the Advanced Photon Source at Argonne National Laboratory (Lemont, IL). The rocks were cored, while submerged in water, into cylinders roughly 1.2 to 1.3 mm in length and 1.5 mm in

diameter using a milling machine and diamond core bit. Each rock was cored in six primary orientations parallel, 45 degrees, and perpendicular to the respective foliation and lineation (Figure 3). The orientation of the foliation and lineation will be referred to in the format: F*- L* where F is the angle between the foliation to the compression direction and L is the angle between the lineation to the compression direction (Figure 3). The D-DIA assembly used in these experiments is a series of concentric hollow cylinders of boron nitride, graphite, and alumina placed in a fired pyrophyllite cube (Figure 4). Crushable alumina pistons were placed above and below the two stacked cores that were separated by a layer of garnet and foils of rhenium and platinum, which were used to identify the ends of the cores in the x-radiographs. The cores were also surrounded by a platinum jacket to chemically isolate them from the surrounding assembly.

The experiments were performed using a D-DIA apparatus (Wang et al., 2003), which uses a six-anvil cubic arrangement (five tungsten anvils and one sintered diamond anvil) to apply equal pressure around a cubic sample. Power to heat the assembly is applied via the upper and lower anvils that are in contact with the ends of the graphite furnace. The upper and lower anvils are also advanced independently of the other four anvils to apply a load to the stacked cylinders. In this study, all the assemblies were deformed at a constant temperature of 900°C, pressure of 2.04 ± 0.28 GPa, and strain rate of ~10^{-6}/s. During deformation, radiographs of the stacked cores and x-ray spectra from the alumina pistons above and below the stacked cores were collected to determine strain, strain rate, pressure, and differential stress.

3.3 Analytical Techniques

After reaching the desired strain, the assemblies were quenched to room temperature over a period of two minutes and slowly depressurized over a two-hour period. The deformed samples were impregnated with epoxy and cut in half to the compression direction and perpendicular to the strike of the foliation. These sample halves were ground using 3.0-micron silicon carbide grit and polished using 0.3-micron Al_2O_3 grit. The polished samples were then analyzed using the scanning electron microscope (SEM) with energy-dispersive X-ray spectroscopy (EDS) at the Department of Geosciences at the University of Akron (Akron, OH). After SEM analysis, double polished thin sections were made by attaching a polished sample half to glass with epoxy. The sample was ground and polished on the glass until it reached the desired thickness of ~30 microns. These thin sections were used for optical analysis under a petrographic microscope to

characterize their optical scale microstructures that help determine the dominant deformation mechanisms.

Mechanical data was analyzed using radiographs of the stacked cores and x-ray spectra collected from the alumina pistons during deformation. The strain and strain rate of each orientation to the foliation and lineation for both the Gneiss Minuti and Moine Thrust quartzite were determined by measuring the change in core lengths in the in-situ radiographs using ImageJ (Figure 5). The pressure and differential stress of each assembly of stacked cores was calculated from the changes in the peak positions of lattice planes located on the collected x-ray spectra from the top and bottom alumina pistons during deformation (Figure 6). These calculations were performed using the computer programs PLOT85, Python, and Polydefix. In addition to mechanical data, microstructural and melt volume analysis was also performed using SEM imaging and by analyzing thin sections under a petrographic microscope or SEM to determine grain size and melt topology. Individual grains and melt pockets/channels were traced from these SEM images and various parameters, such as area and diameter, were determined using Adobe Photoshop and ImageJ. For this study, I define melt pockets as areas of melt between grains that have a low aspect ratio and melt channels as areas of melt with a high aspect ratio (Figure 7). However, the difference between melt pockets and channels is more qualitative. Thin sections of the Gneiss Minuti and Moine Thrust quartzite were also analyzed under cross-polarized light to characterize the optical microstructures produced by the dominant deformation mechanisms that operated during the experiments.

4. Results

4.1 Mechanical Data

4.1.1 Gneiss Minuti

Four sets of stacked Gneiss Minuti cores were deformed using the D-DIA apparatus at a constant temperature (T) of 900°C, pressure (P) of 1.90 ± 0.25 GPa, and ($\dot{\varepsilon}$) strain rate of ~10^{-6}/s (Table 1). Total strains of the cores ranged from 19% to 45% (Table 1 and Figure 8). In all the experiments, differential stresses increased rapidly over the first ~10% strain then deformed at a relatively constant stress (Figure 9). The average differential stress for all four experiments ranged from 1.01 to 1.17 GPa during constant stress deformation.

4.1.2 Moine Thrust Quartzite

Three stacked cores of the Moine Thrust quartzite were deformed using the D-DIA apparatus at similar conditions as the Gneiss Minuti experiments (T = 900°C, P = 2.22 ± 0.26 GPa, and ($\dot{\varepsilon}$) = ~10^{-6}/s) (Table 1). The total strains of the quartzite cores ranged from roughly 16% to 45% (Table 1 and Figure 10). The differential stresses increased rapidly over the first ~10% strain then deformed at a relatively constant stress. The average differential stress ranged from 1.28 to 1.61 GPa during constant stress deformation (Figure 11).

4.2 Microstructures

4.1.1 Gneiss Minuti

Deformation throughout the Gneiss Minuti cores were homogenous (Figure 12). Optical microstructures in the quartz and plagioclase of the samples includes undulatory extinction and deformation lamellae, and no evidence of brittle behavior was observed. Biotite grains sometimes had kinks or were sheared depending on their orientation relative to the compression direction.

Melt was present in all cores and was located in a mixture of melt pockets and channels cutting through single grains and along grain boundaries parallel to the compression direction regardless of foliation and/or lineation orientation. The melt concentration in the cores of Gneiss Minuti ranged from roughly 1 to 4 vol% (Table 1). Composition of the melt was analyzed using energy-dispersive X-ray spectroscopy (EDS), and the melt contains Si, Al, Ca, Na, and K (Figure 13). All cores with foliation oriented 45 degrees and perpendicular and most cores parallel to the compression direction had similar melt contents (~1 to 3 vol%) and show similar melt topology (Table 1 and Figure 14). Melt was observed as channels crossing and connecting the length of single grains in all cores with foliation oriented 45 degrees and perpendicular and in two cores with foliation oriented parallel (Figure 14). In one of the foliation parallel cores (F0-L0), the core which also had the highest melt fraction, melt was observed in channels that extended along several grains (Figure 15).

4.1.2 Moine Thrust Quartzite

Deformation in the Moine Thrust quartzite was relatively homogenous, but localization along muscovite-rich bands did occur in the core with foliation 45 degrees to the compression direction (Figure 16). Optical microstructures observed in quartz included undulatory extinction,

deformation lamellae, and grain boundary bulging, and the muscovite grains were sometimes kinked or sheared (Figure 16).

Melt topology and concentration was also determine in the Moine Thrust quartzite samples. At T = 900°C, melt content within these samples ranged from 0.6 to 1.2 vol%, and distinguishable melt was observed in the quartzite samples regardless of the orientation to foliation and/or lineation. All the cores had a similar melt topology of small, scattered melt pockets vertical to the compression direction (Table 1, Figure 17, and Figure 18). However, these pockets were usually not evenly distributed and were random throughout the sample with some localization seen in the outer portions of the cores. EDS was not performed for the Moine Thrust quartzite samples because the present melt pockets/channels were too small to collect accurate results.

5. Discussion

5.1 Microstructures

At a T = 900°C, P = ~2 GPa, and $\dot{\varepsilon} = \sim 10^{-6}$/s, the framework of both the Gneiss Minuti and the Moine Thrust quartzite deformed by crystal plastic mechanisms. The microstructures included undulatory extinction and deformation lamellae in the quartz and plagioclase in the Gneiss Minuti as well as undulatory extinction, deformation lamellae, and grain boundary bulging of the quartz in the Moine Thrust quartzite (Figure 12 and Figure 16). The biotite and muscovite from each rock, respectively, were sometimes kinked or sheared. These microstructures are consistent with deformation by dislocation creep (Hirth and Tullis, 1992). Some of these microstructures were seen in the starting material, such as undulatory extinction in the Gneiss Minuti and undulatory extinction/grain bulging in the Moine Thrust quartzite; however, they were more exaggerated and frequent following deformation. Additionally, the deformation lamellae were only observed in the deformed samples for both rocks. Moreover, deformation was homogenous in all the cores except the Moine Thrust quartzite F45-L45 core, where strain localized along bands of interconnected muscovite (Figure 16).

5.2 Melt topology

Melt present within all the Gneiss Minuti samples appears to have a similar melt topology of scattered melt pockets and vertical, single grain length melt channels regardless of the foliation and/or lineation orientation (Figure 14). The presence of melt channels cross-cutting

grains within the samples indicates brittle behavior likely induced by high local melt pore pressure. The siliceous nature of the Gneiss Minuti melt, which is similar to that of a granitic composition, likely caused high local pore pressure that induced vertical cracking through grains because the extremely viscous melt could not migrate fast enough along grain boundaries to relieve this pore pressure. The only sample to show interconnected melt channels across multiple grain boundaries is the F0-L0 sample (Figure 15). This sample has the largest melt content (3.74%) of all the samples in both the Gneiss Minuti and the Moine Thrust quartzite (Table 1). All orientations of the Moine Thrust quartzite, similar to the cores of Gneiss Minuti, had similar melt topology with melt fractions ranging from 0.6 to 1.2 vol% (Table 1, Figure 17, and Figure 18). The melt, however, was usually only observed in small, scattered pockets with occasional vertical melt channels. These results from both the Gneiss Minuti and Moine Thrust quartzite suggest that foliation and/or lineation orientation does not have a significant effect on melt interconnectivity, but rather melt fraction plays a larger role in melt interconnectivity, segregation, and migration.

Differences in composition between the Gneiss Minuti and Moine Thrust quartzite likely caused the difference in viscosity and melt fraction of the two rocks. At the conditions of the experiments, I expected the Gneiss Minuti (Eq. 1) and Moine Thrust quartzite (Eq. 2) to form melt by the reactions:

$$Bt + Qtz + Pl \rightarrow Melt + Gt + Opx + Kfs \quad \text{Eq. 1}$$

and

$$Mus + Qtz \rightarrow Melt + Sil + Bt + Kfs \quad \text{Eq. 2}$$

where Bt is biotite, Qtz is quartz, Pl is plagioclase, Gt is garnet, Opx is orthopyroxene, Kfs is potassium feldspar, Mus is muscovite, and Sil is silica. These reactions cause a vol% increase of 30% and ~7% (Rushmer, 2001), respectively, which caused cataclastic behavior in the Holyoke and Rushmer (2002) experiments. My experiments were performed at similar temperatures to their study but at higher pressures; this difference of pressure likely affects the melt reaction, causing lower melt fractions as observed in my experiments (Table 1). A lower melt fraction means lower pore pressure or more limited zones of high pore pressure. The high pressure in my experiments also inhibits brittle behavior and makes the dislocation creep of quartz easier (Tullis and Yund, 1977; Hirth and Tullis, 1994). The absence of the solid by-products and cataclastic

behavior in this study indicates that the melting reaction in the samples may be wet melting, rather than the predicted reactions.

5.3 Viscous Anisotropy

The relative strengths between the foliation/lineation orientations within the Gneiss Minuti and the Moine Thrust quartzite under crystal plastic conditions were determined by investigating the viscous anisotropy between all the cores. Each core was deformed at a slightly different combination of strain rate ($\dot{\varepsilon}$) and differential stress (σ_{diff}), so direct comparison is not possible, unless we compare viscosity. The viscosity (η) can be found for each core orientation using stress and strain data collected during deformation in the equation:

$$\eta = \frac{\sigma_{diff}}{\dot{\varepsilon}} \qquad \text{Eq. 3}$$

where η is the viscosity (GPa*s), σ_{diff} is the differential stress (GPa), and $\dot{\varepsilon}$ is the strain rate (1/s). An absence or decrease of viscous anisotropy between the orientations indicates that melt formation dominates the strength of the rock; however, if the cores are significantly different in viscosity, the foliation/lineation present within the rock is still controlling the overall strength.

All cores of the Gneiss Minuti except one (F0-L45) have similar viscosities (~$2*10^4$ GPa*s) and the melt content within these cores ranges from 1 to 4 vol% (Table 1 and Figure 19). However, the viscosity of the F0-L45 core is almost twice that of the other Gneiss Minuti cores with different orientations (Figure 19 and Figure 20). The melt content in this core is lower than most of the other cores (1 vol% vs. >2 vol%), which suggests that foliation and/or lineation still controls the strength of this core, and melt is controlling the strength in the other cores with higher melt contents (Table 1). However, the F0-L90 core, which also has a low melt content (1.1%) has a similar viscosity to the cores with higher melt contents.

Not all orientations of the Moine Thrust quartzite cores have similar viscosities, but the melt contents of these cores are more consistent (0.6-1.2 vol%) than those in the Gneiss Minuti (1-4 vol%). The general pattern of viscosities is consistent with rocks that show viscous anisotropy. The core in the F90-L90 orientation is the strongest with those of foliation 45 degrees being weakest and those with the foliation parallel intermediate in strength; there is an exception with the core in the F0-L0 orientation, which is the weakest of all the cores (Figure 19 and Figure 20). This more pronounced viscous anisotropy and low melt content within the quartzite suggests that foliation and/or lineation still had some influence on the rock strength, which

explains why the F90-L90 core, typically the strongest foliation/lineation orientation, shows a much larger viscosity than the cores at other orientations (Figure 20).

The results from both the Gneiss Minuti and Moine Thrust quartzite experiments indicate that the influence of foliation and/or lineation orientation on strength is negligible at melt fractions greater than 2 vol%. The decrease in viscous anisotropy as melt is introduced to the system is likely linked to how partial melting has been observed to disrupt the framework within source rock that supports applied loads (Rushmer, 2001).

6. Conclusions

To investigate the influence of foliation/lineation orientation and partial melting on rock strength evolution as well as examine the effects of foliation/lineation and source rock composition on melt migration, cores of the Gneiss Minuti and the Moine Thrust quartzite were deformed at six primary orientations parallel, 45 degrees, and perpendicular to the foliation and lineation. The results indicate that in rocks with a melt fraction greater than ~1 to 2 vol%, the influence of the orientation of foliation and lineation on rock strength begins to decrease (i.e., rock strength becomes isotropic). In addition, foliation and lineation orientation have less of an influence on granitic melt interconnectivity than melt fraction.

7. Acknowledgments

All in all, I would like to thank Dr. Caleb Holyoke, my advisor, for his guidance, advice, and support through this project as well as throughout my undergraduate career. I would also like to thank Haiyan Chen for her assistance with experiments at the Advanced Photon Source at Argonne National Laboratory, and Tom Quick for his assistance in operating the scanning electron microscope. Additionally, thank you to Dr. John Peck and Dr. Molly Witter for agreeing to be my readers for this project and offering constructive feedback. Finally, I would like to thank my peers Maria Razo, Jake Waller, and JJ Kullberg for their help and support in various activities relating to this project.

8. References

Braccia, C., and Holyoke, C. W., 2019, Transient Effects of a Pre-existing Lattice Preferred Orientation on the Strength of a Foliated Quartzite, Abstract T41A-07 presented at 2019 Fall Meeting, AGU, Washington, D.C., 9-13 Dec.

Brown, M., 2007. Crustal melting and melt extraction, ascent and emplacement in orogens: mechanisms and consequences. Journal of the Geological Society 164, 709–790.

Bürgmann, R., and Dresen, G., 2008. Rheology of the Lower Crust and Upper Mantle: Evidence from Rock Mechanics, Geodesy, and Field Observations. Annual Review of Earth and Planetary Sciences 36, 531–567.

Dell 'Angelo, L. N., and Tullis, J., 1988. Experimental deformation of partially melted granitic aggregates. Journal of Metamorphic Geology 6, 495–515.

Gottschalk, R. R., Kronenberg, A. K., Russel, J. E., and Handin, J., 1990. Mechanical Anisotropy of Gneiss: Failure Criterion and Textural Sources of Directional Behavior. Journal of Geophysical Research 95, 21613–21634.

Hansen, L.N., Zimmerman, M.E., and Kohlstedt D.L., 2012. Laboratory measurements of the viscous anisotropy of olivine aggregates. Nature 492, 415–419.

Hirth, G., and Tullis, J., 1992. Dislocation creep regimes in quartz aggregates. Journal of Geophysical Research 14, 145–159.

Hirth, G., and Tullis, J., 1994. The brittle-plastic transition in experimentally deformed quartz aggregates. Journal of Geophysical Research 99, 11731–11747.

Holyoke, C.W., and Rushmer, T., 2002. An experimental study of grain scale melt segregation mechanisms in two common crustal rock types. Journal of Metamorphic Geology 20, 493–512.

Law, R.D., Casey, M., and Knipe, R. J., 1986. Kinematic and tectonic significance of microstructures and crystallographic fabrics within quartz mylonites from the Assynt and Eriboll regions of the Moine thrust zone, NW Scotland, Transactions of the Royal Society of Edinburgh. Earth Sciences 77, 99–125.

Rushmer, T., 2001. Volume change during partial melting reactions: implications for melt extraction, melt geochemistry and crustal rheology. Tectonophysics 342, 389–405.

Tullis, J., and Yund, R.A., 1977. Experimental deformation of Dry Westerly Granite. Journal of Geophysical Research 82, 5705–5718.

Wang, Y., Durham, W.B., Getting, I.C., and Weidner, D.J., 2003. The deformation-DIA: A new apparatus for high temperature triaxial deformation to pressures up to 15 GPa. Review of Scientific Instruments 74, 3302–3011.

Zurbriggen, R., Kamber, B. S., Handy, M. R., and Naegler, T. F., 1998. Dating synmagmatic folds; a case study of Schlingen structures in the Strona-Ceneri Zone (Southern Alps, northern Italy). Journal of Metamorphic Geology 16, 403–414.

Table 1. Data for the Gneiss Minuti and Moine Thrust quartzite experiments.

Sample	Material	Orientation of Foliation and Lineation to Length of Core	Temperature (T) C°	Pressure (P) GPa	Differential Stress (σ) GPa	Total Strain (ε) %	Strain Rate (ε̇) $*10^{-6}$/s	Melt Fraction %
GM_004	Gneiss Minuti	F45-L45	900	2.02	1.02	28.52	5.27	3.26
		F90-L90				32.83	5.81	2.53
GM_005	Gneiss Minuti	F0-L0	900	1.54	1.01	30.15	5.55	3.74
		F90-L90				23.26	4.21	2.50
GM_016	Gneiss Minuti	F45-L90	900	2.07	1.17	35.56	5.76	2.17
		F90-L90				32.31	4.96	2.13
GM_017	Gneiss Minuti	F0-L90	900	1.99	1.12	44.76	7.29	1.10
		F0-L45				19.23	3.22	1.03
GM_013	Moine Thrust quartzite	F45-L45	900	2.41	1.61	34.82	5.22	1.19
		F90-L90				15.85	2.25	0.89
GM_021	Moine Thrust quartzite	F45-L90	900	1.92	1.40	29.60	5.10	0.60
		F0-L90				23.58	3.85	0.86
GM_022	Moine Thrust quartzite	F0-L45	900	2.32	1.28	24.32	3.78	0.58
		F0-L0				44.83	7.00	0.55

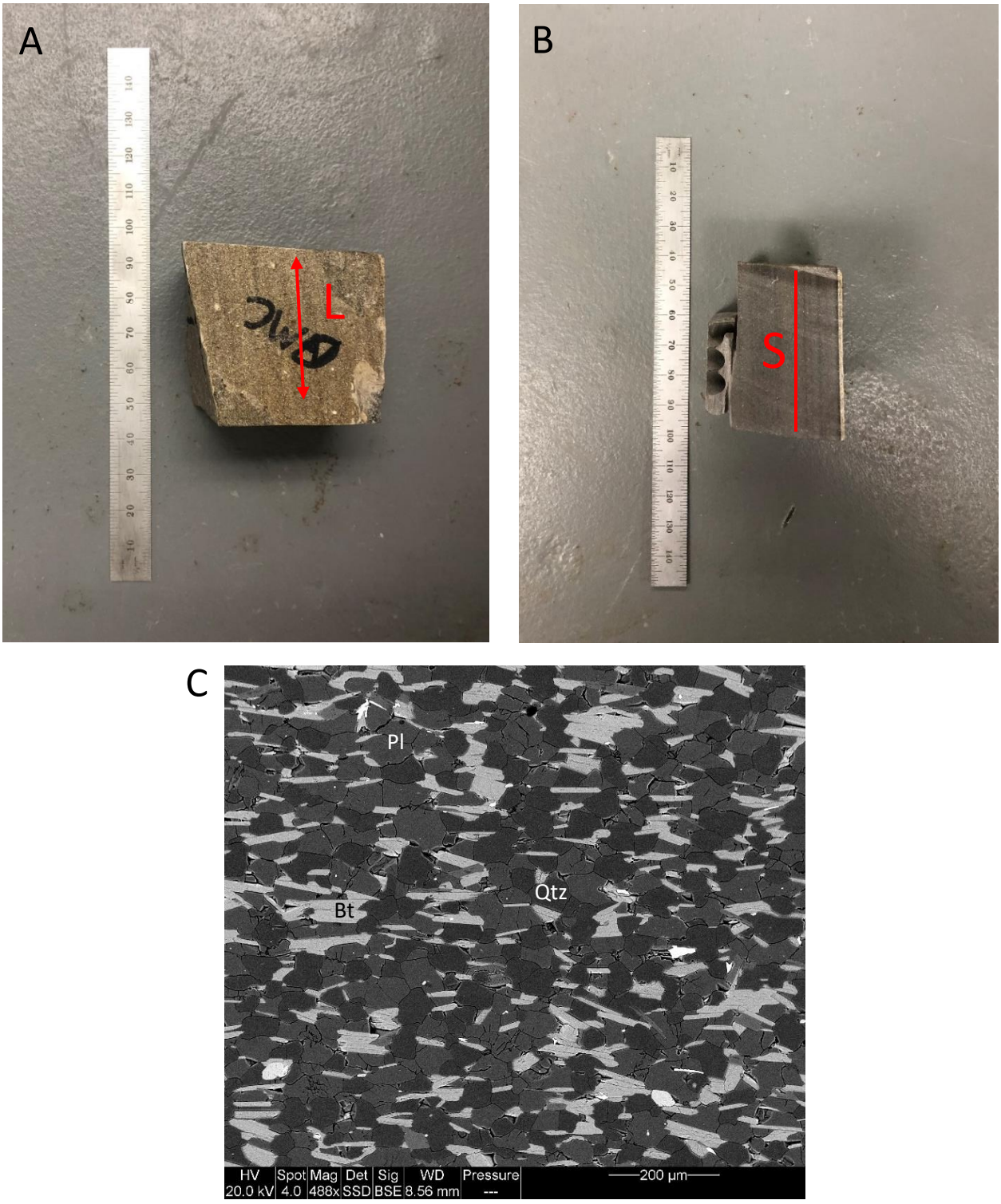

Figure 1. Gneiss Minuti block showing the lineation, L (A), which lies on the foliation plane, S, (plane parallel to page in A, plane perpendicular to page in B). Scale is in millimeters (#10 = 10 mm). The starting material is composed of quartz, plagioclase, and biotite (C).

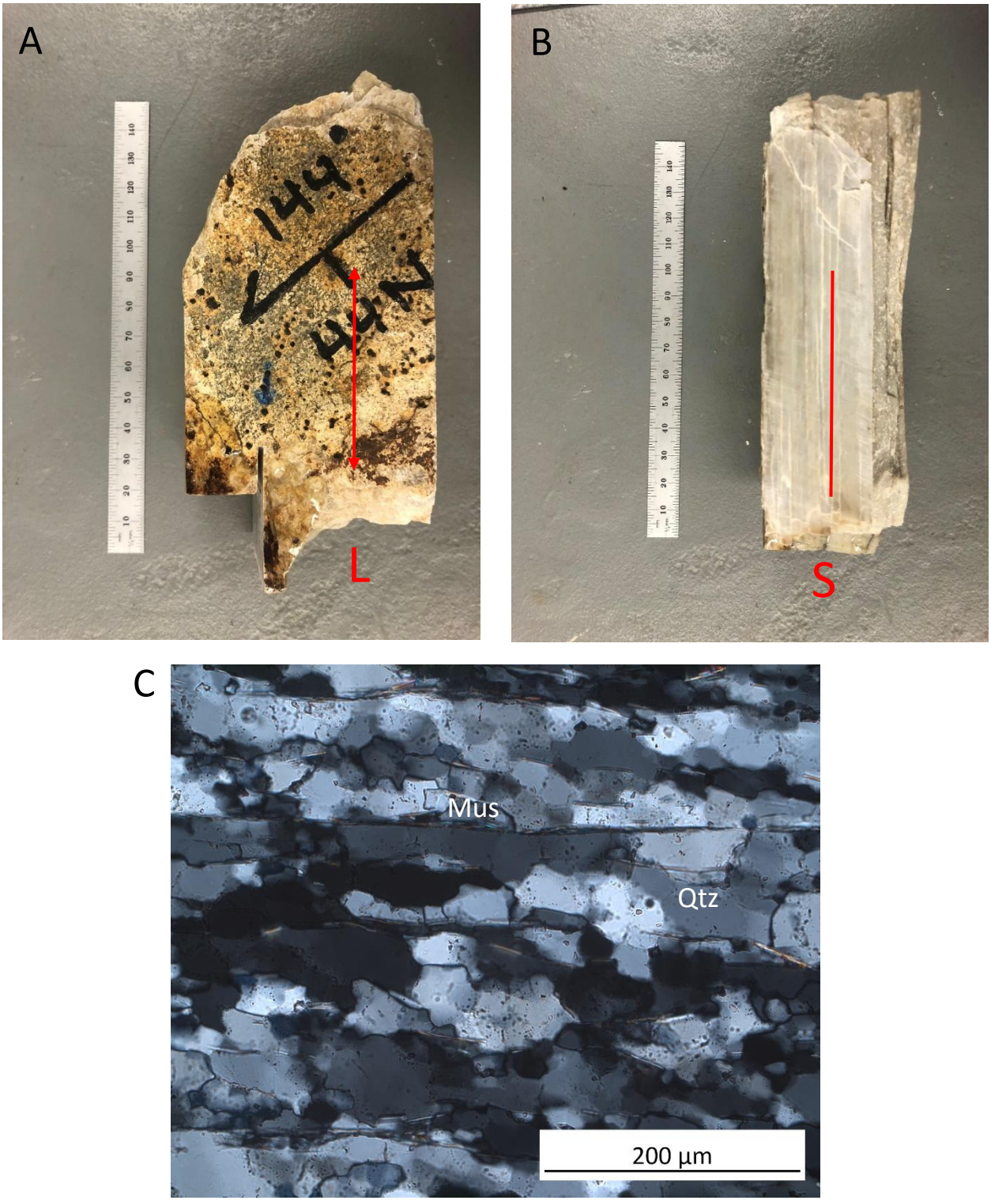

Figure 2. Moine Thrust quartzite block showing the lineation, L (top image), which lies on the foliation plane, S, (plane parallel to page in A, plane perpendicular to page in B. Scale is in millimeters (#10 = 10 mm). The starting material is composed of quartz and muscovite (C).

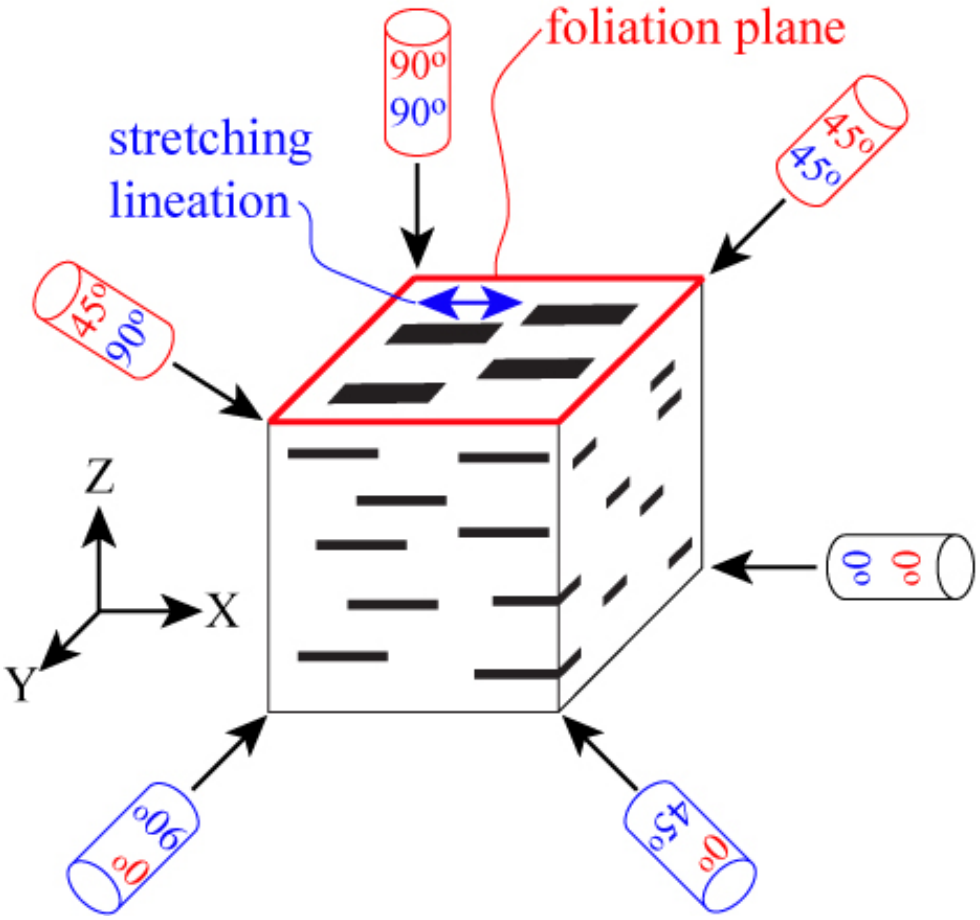

Figure 3. Cores for experiments in this study were collected at six primary orientations relative to the foliation and lineation. The red top number represents the core angle to the foliation, and the blue bottom number represents the core angle to the lineation. Drawing provided by Dr. Holyoke.

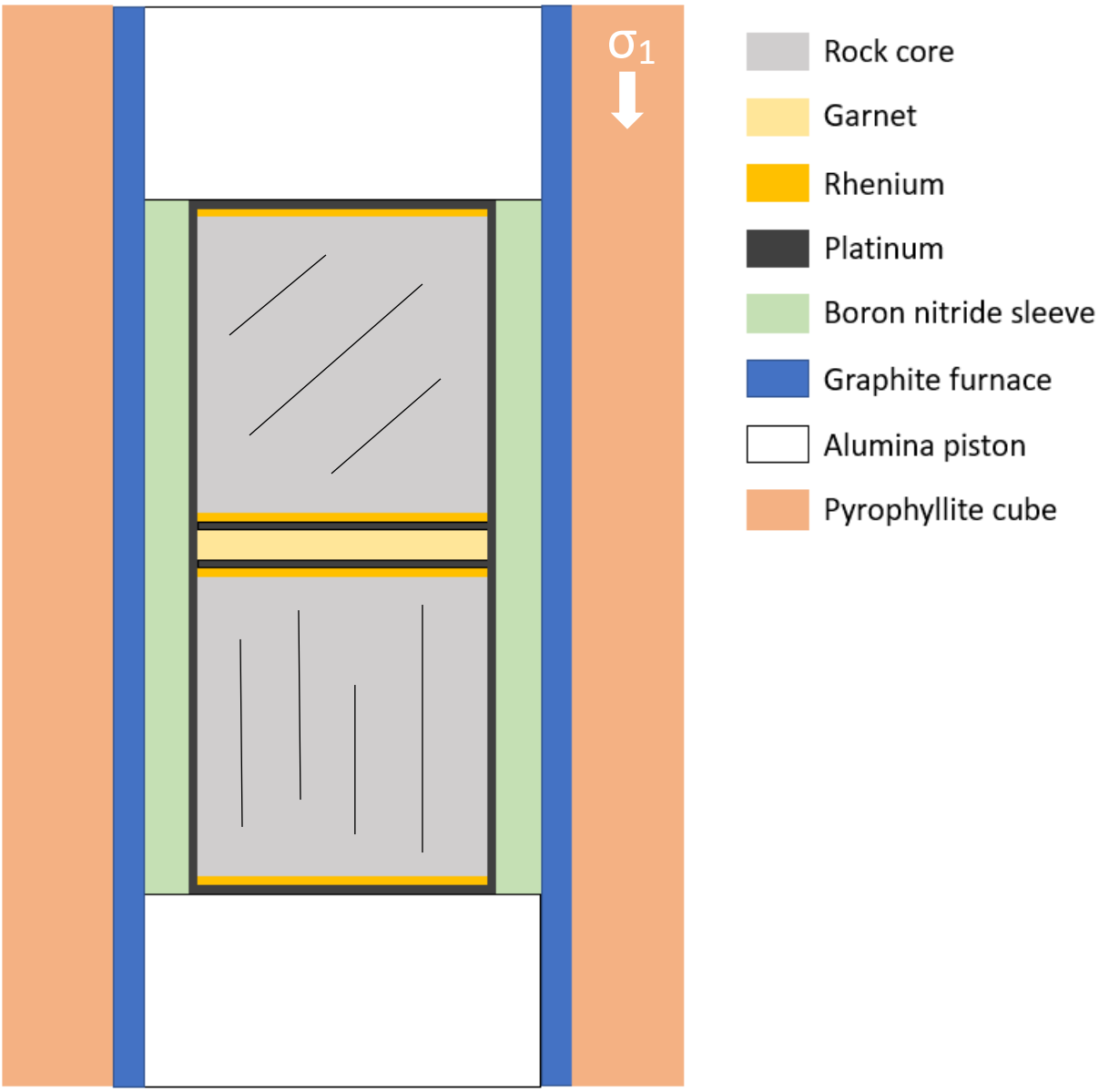

Figure 4. Schematic of the D-DIA assembly used to deform the Gneiss Minuti and Moine Thrust quartzite.

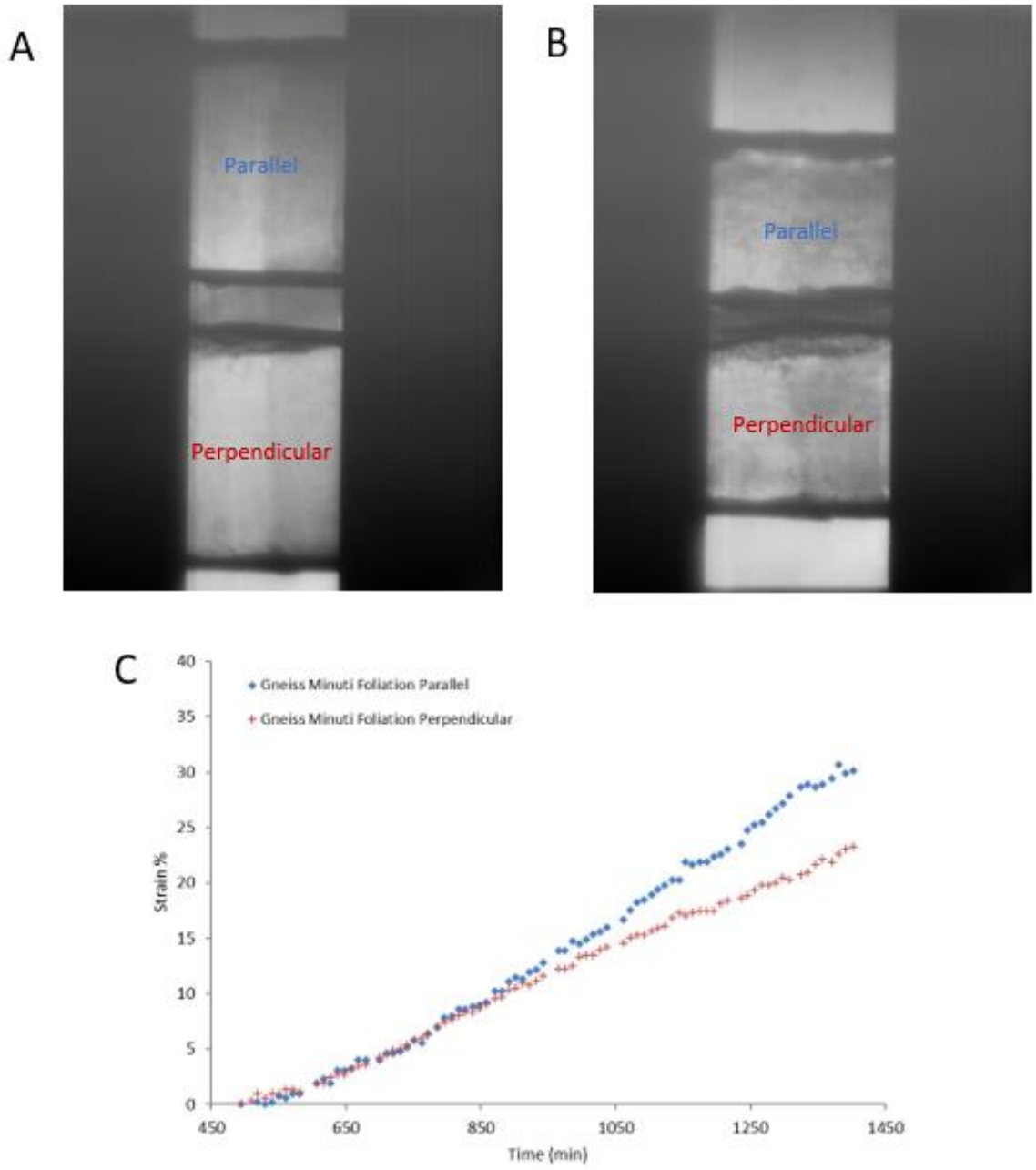

Figure 5. The X-radiographs show cores (A) before and (B) after deformation in the D-DIA apparatus, and (C) the bottom graph is an example of strain data used to highlight the contrast in strain rate between cores of different foliation orientations.

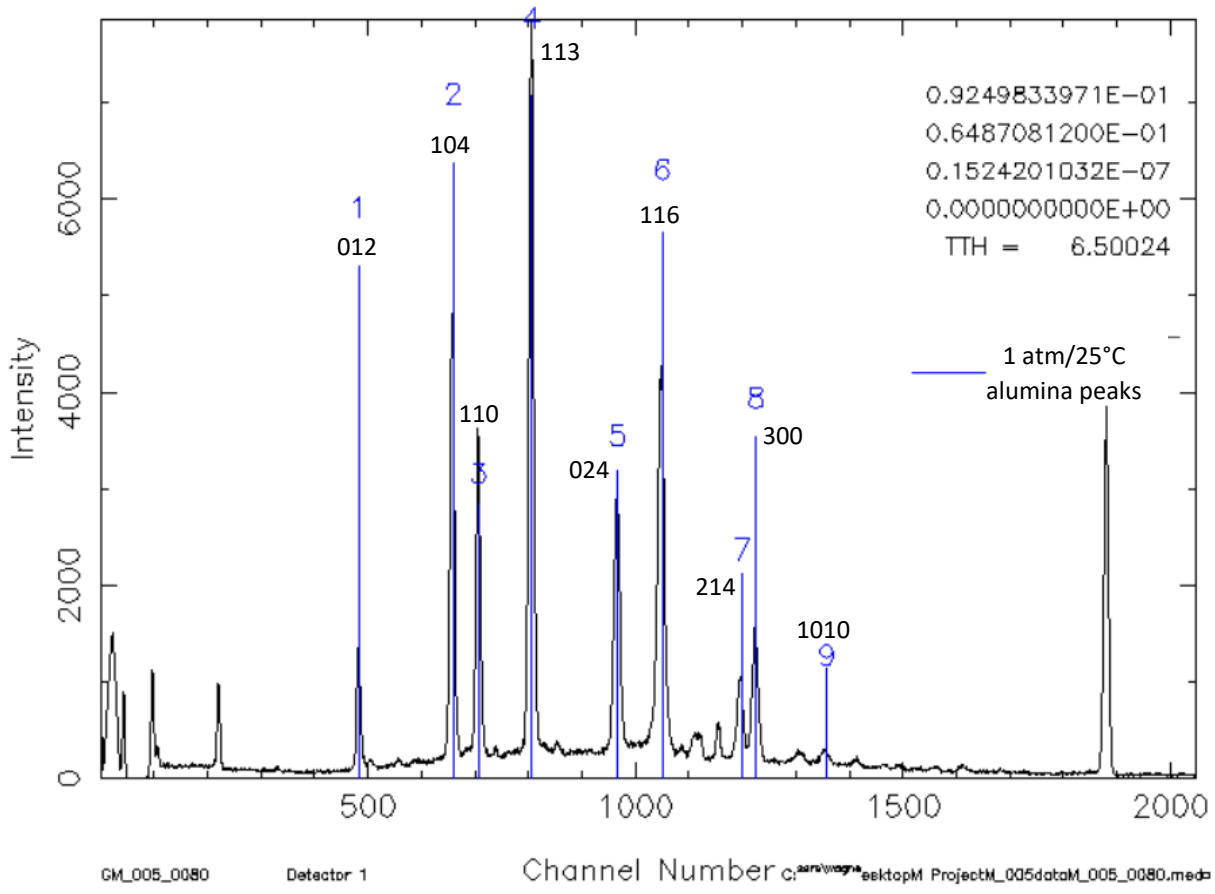

Figure 6. Peaks of Al_2O_3 in X-ray spectra collected from the top and bottom pistons during deformation (with 1atm/25°C alumina peaks indicated in blue and lattice planes labeled) are shifted slightly to the left due to compression of the crystal lattice. The channel number refers to the energy, which is found by determining 2θ in Bragg's Law ($n\lambda = 2d\sin\theta$). These peak shifts are used to determine differential stresses during deformation of the Gneiss Minuti and Moine Thrust quartzite.

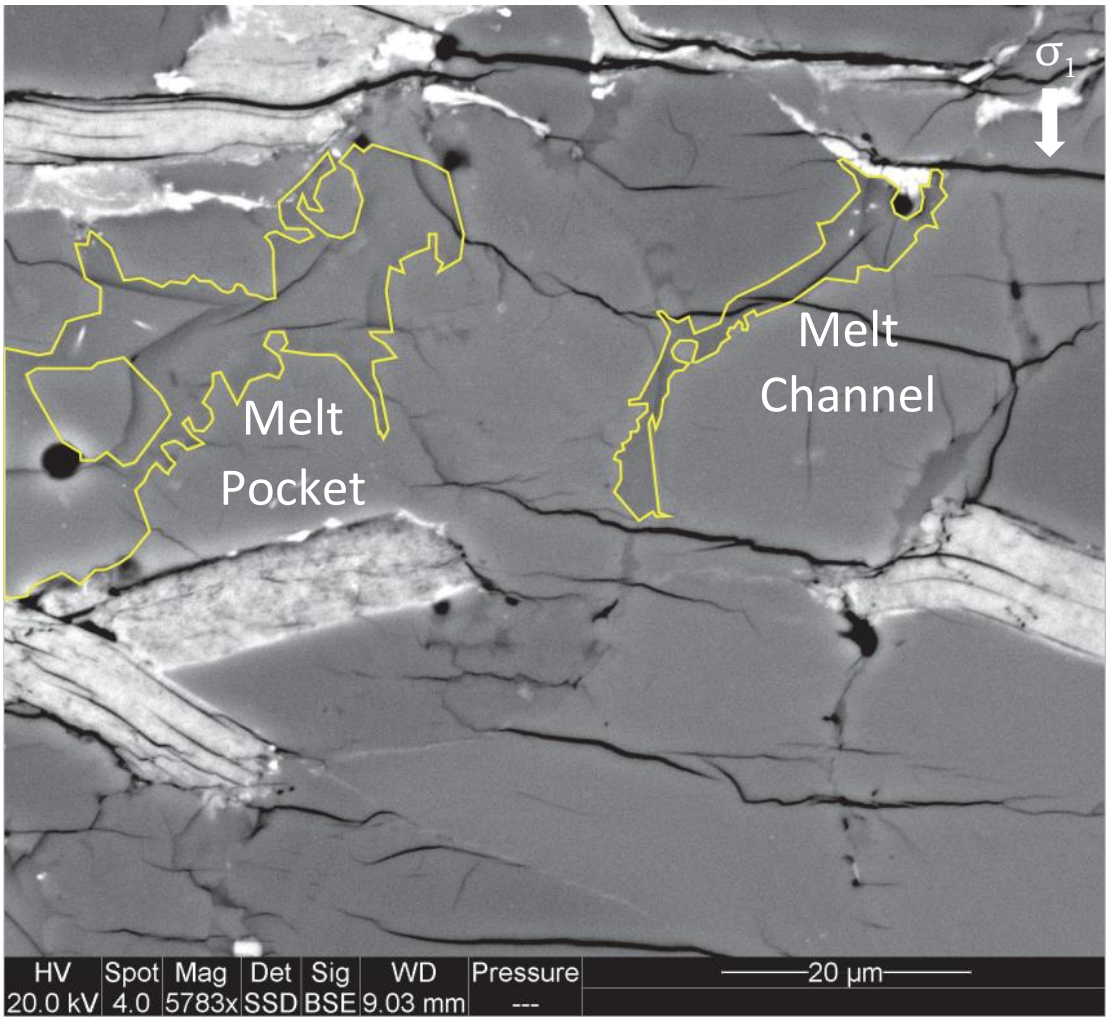

Figure 7. An SEM image showing an outline of a melt pocket and melt channel for the differentiation used in this study.

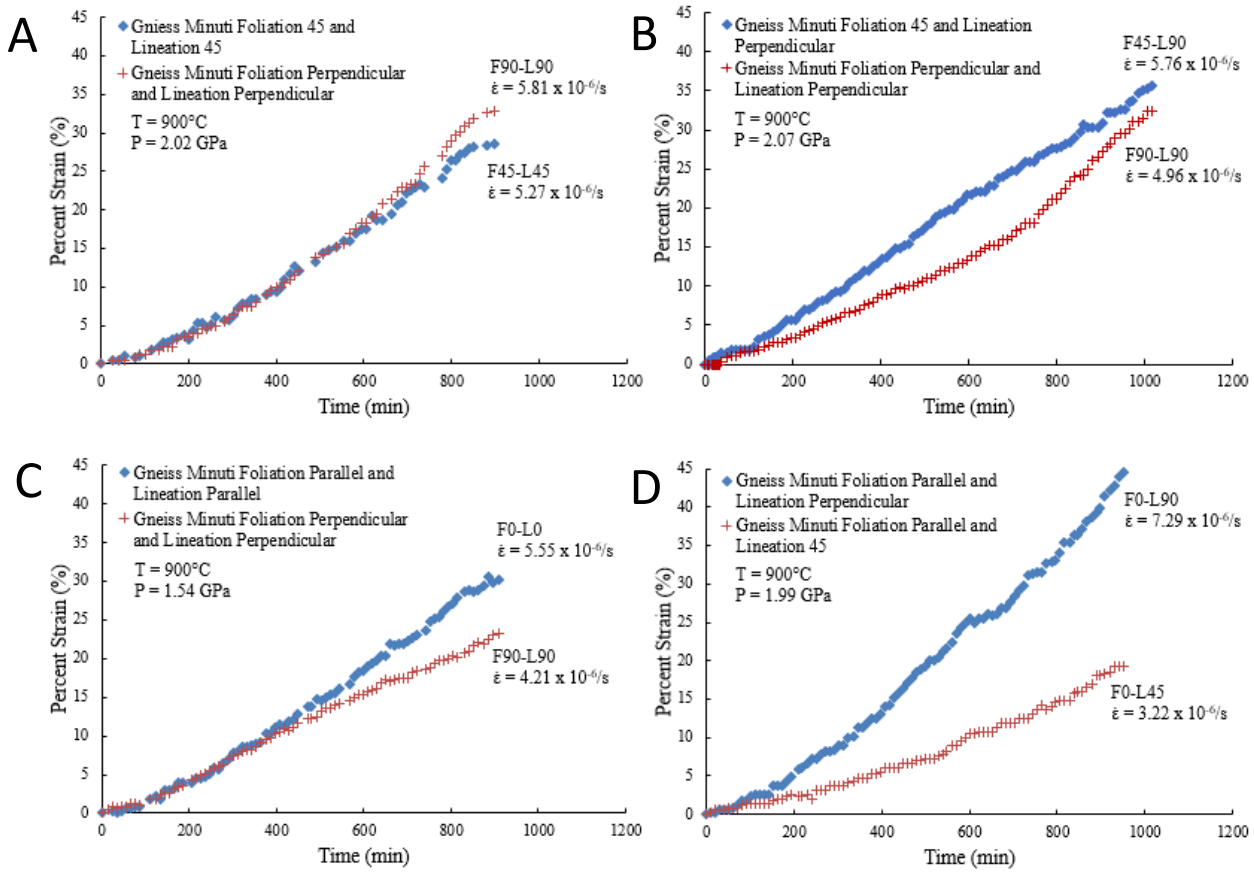

Figure 8. The strain rates for each foliation and lineation orientation of the Gneiss Minuti cores. The strain rates can be used as an estimation of the strength of each orientation relative to each other.

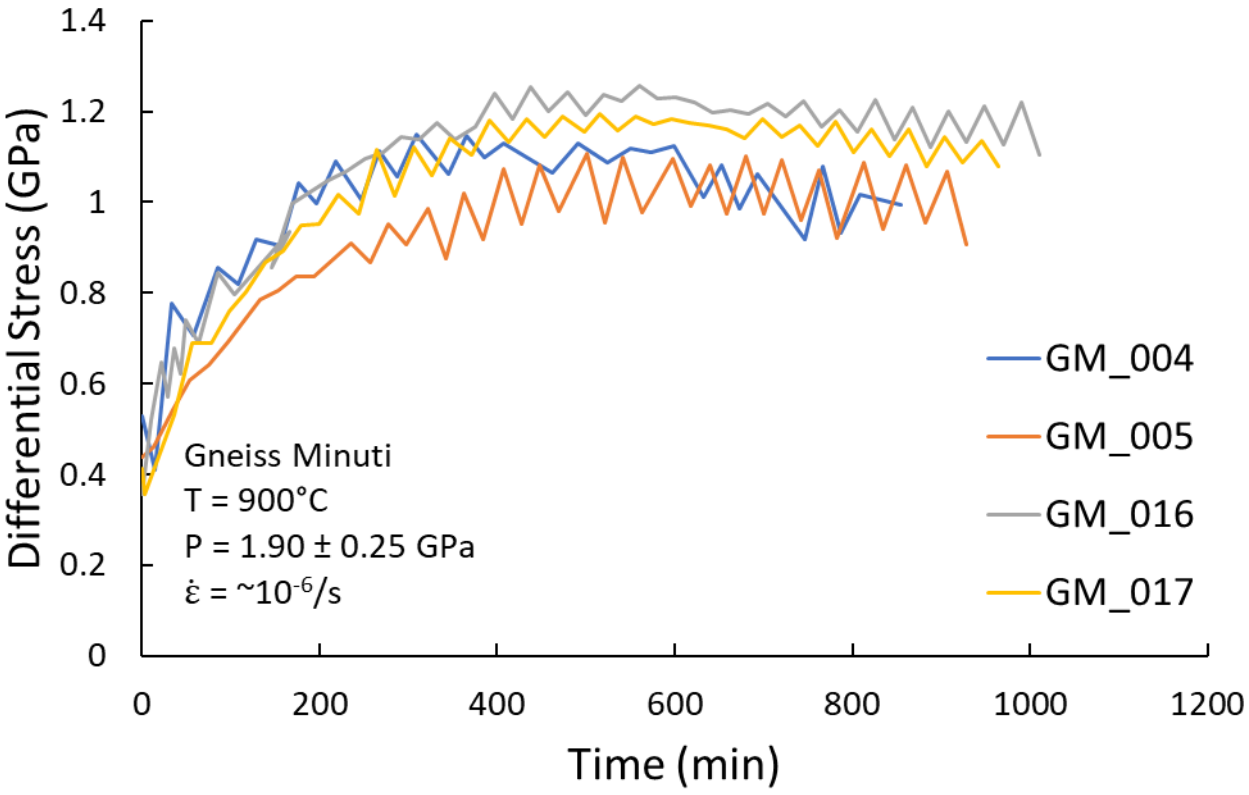

Figure 9. The average differential stress of all four Gneiss Minuti experiments was constant after reaching the peak stress at a strain of ~10% and ranged from roughly 0.9 to 1.2 GPa. The sawtooth pattern is a result of the X-ray spectra, that is used to calculate differential stresses, being collected from both the top and bottom alumina pistons.

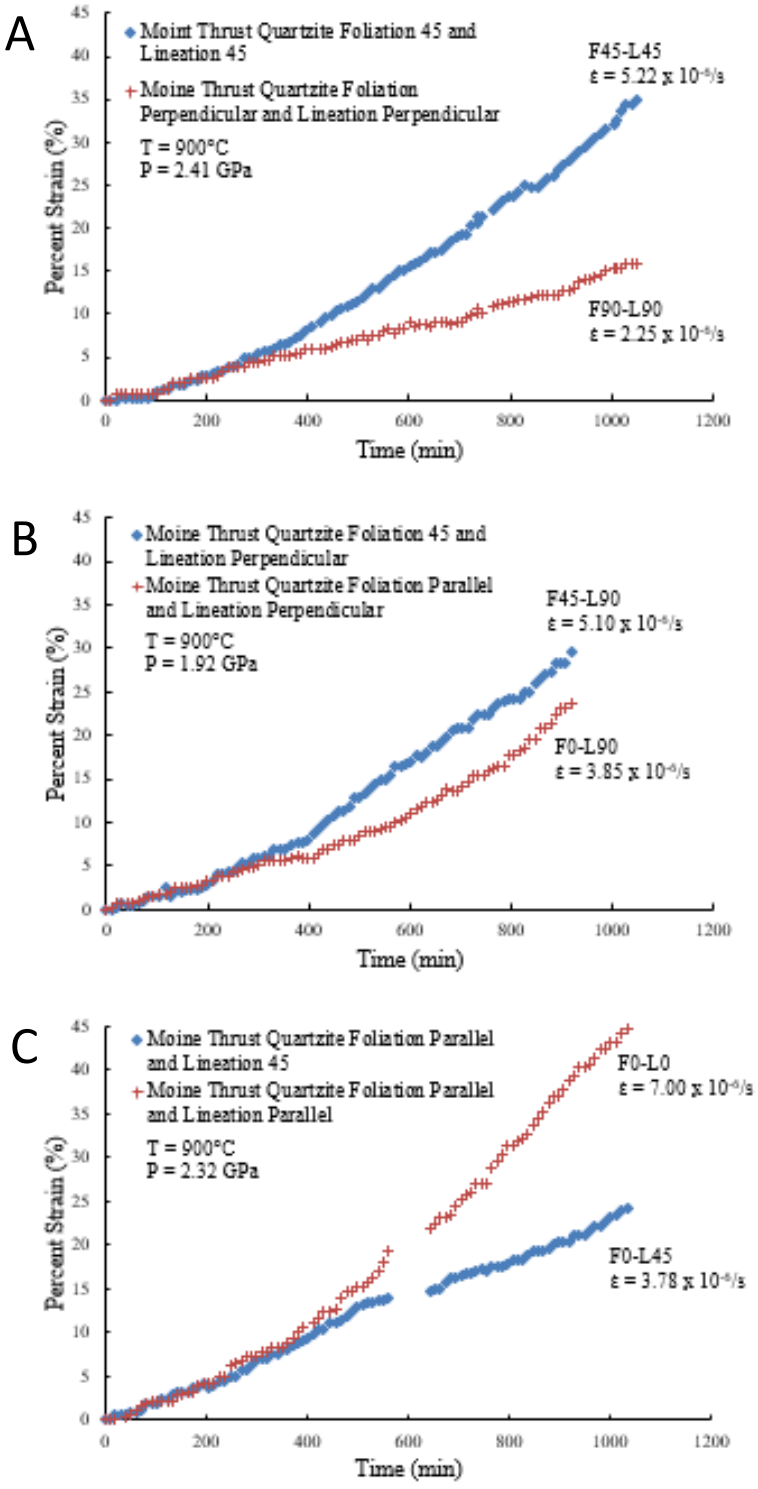

Figure 10. The strain rates for each foliation and lineation orientation of the Moine Thrust quartzite cores. The strain rates can be used as an estimation of the strength of each orientation relative to each other.

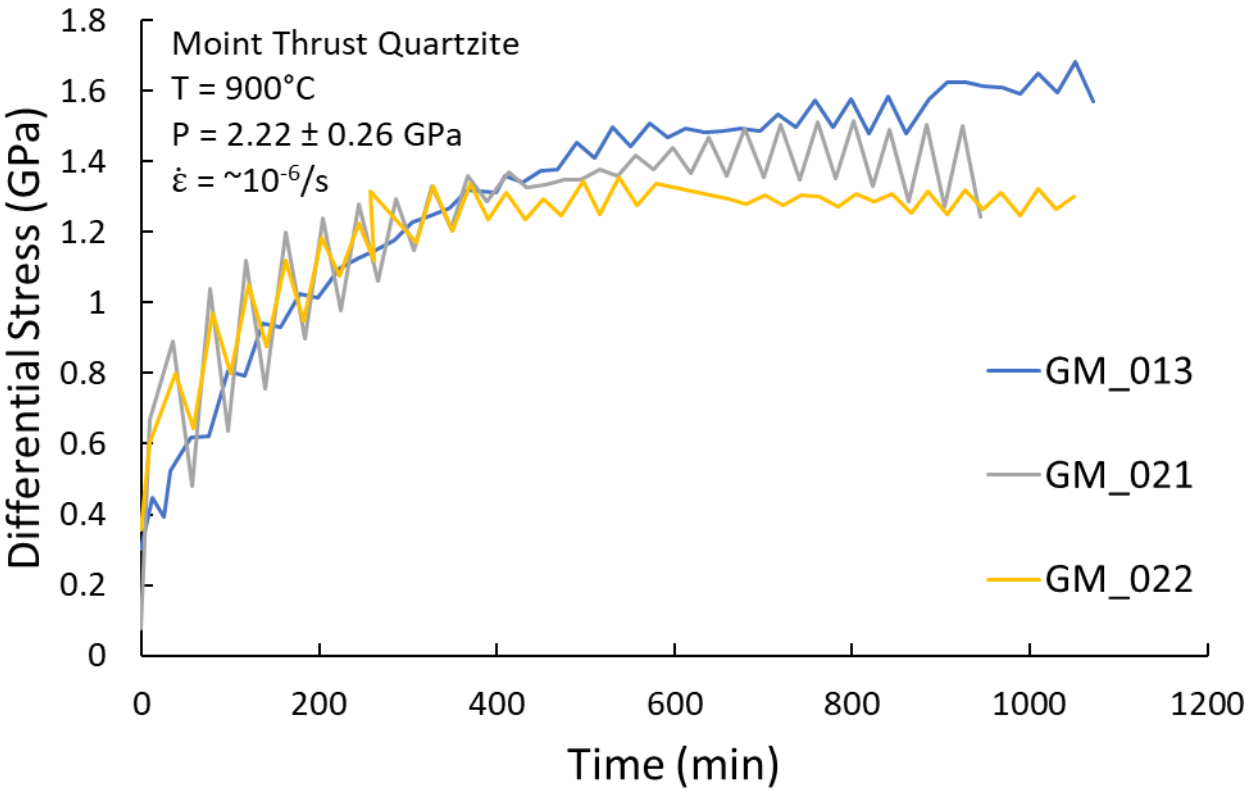

Figure 11. The average differential stress of all three Moine Thrust quartzite experiments was constant after reaching the peak stress at a strain of ~10% and ranged from roughly 1.2 to 1.6 GPa. The sawtooth pattern is a result of the X-ray spectra, that is used to calculate differential stresses, being collected from both the top and bottom alumina pistons.

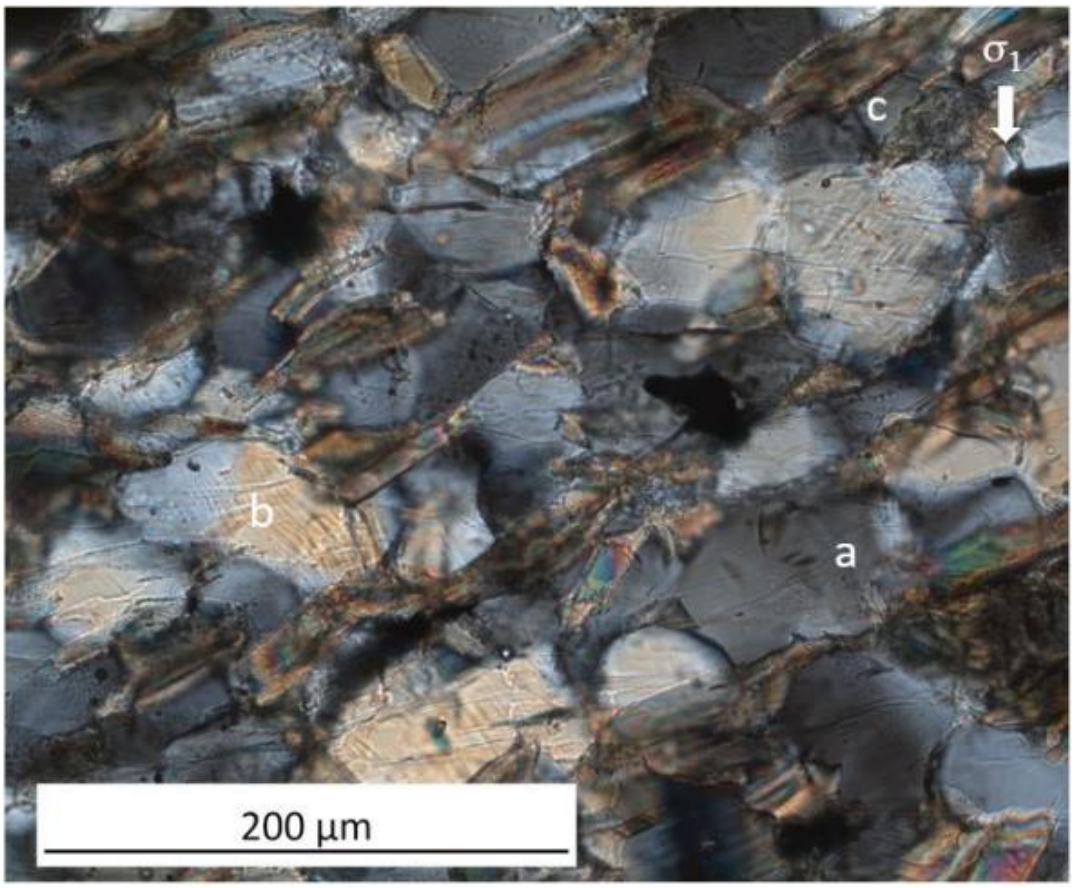

Figure 12. Optical image of deformed Gneiss Minuti showing undulatory extinction (a), deformation lamellae (b) in the quartz and plagioclase, and shear/kinked biotite (c) (Experiment information: F45-L45, T = 900°C, P = 2.02 GPa, ε = 28.52%, and $\dot{\varepsilon}$ = 5.37 x 10^{-6}/s).

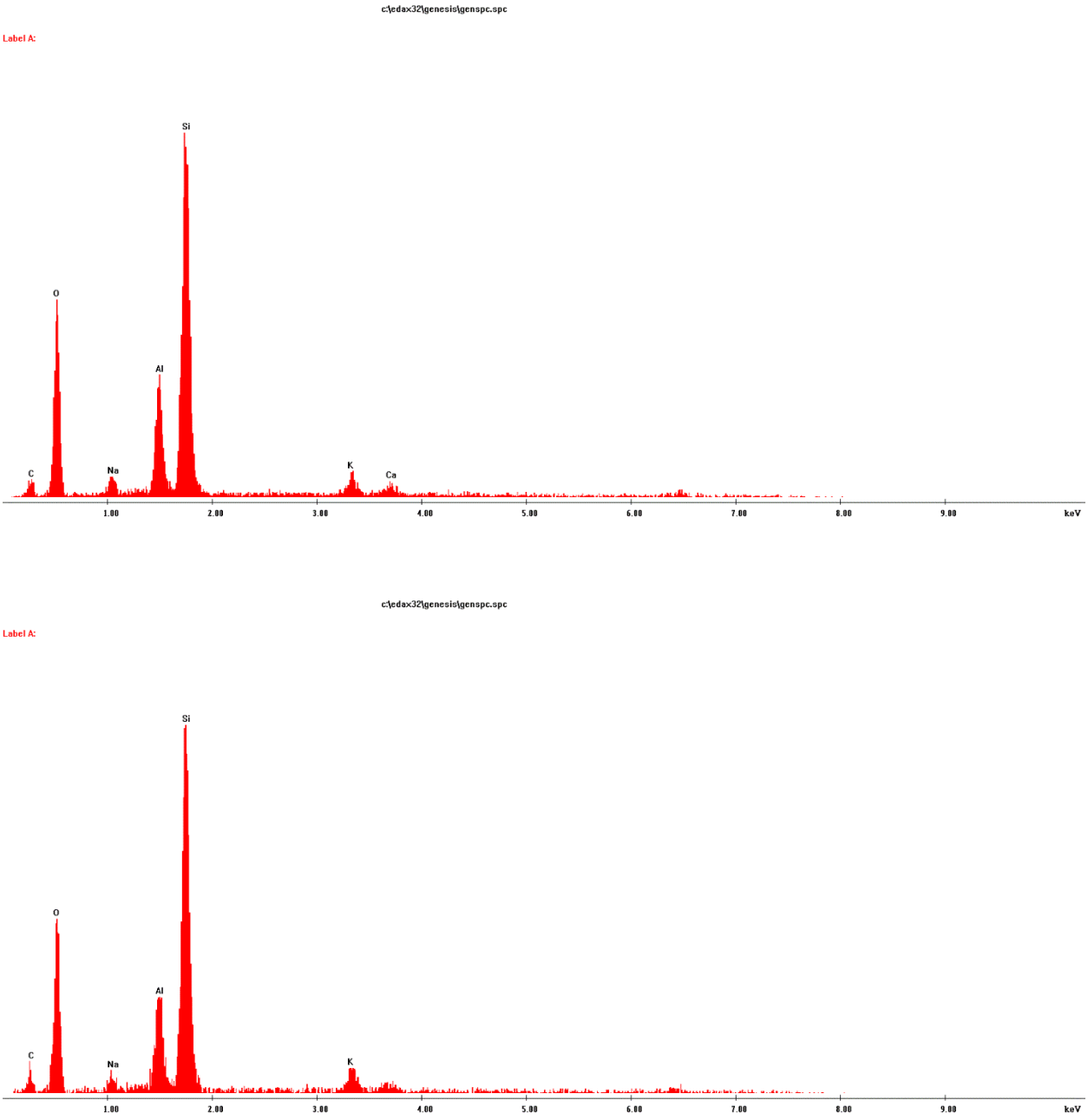

Figure 13. EDS analysis of melt in the deformed Gneiss Minuti samples. The melt contains silica, aluminum, calcium, sodium, and potassium. The x-axis is energy, and the y-axis is counts (concentration).

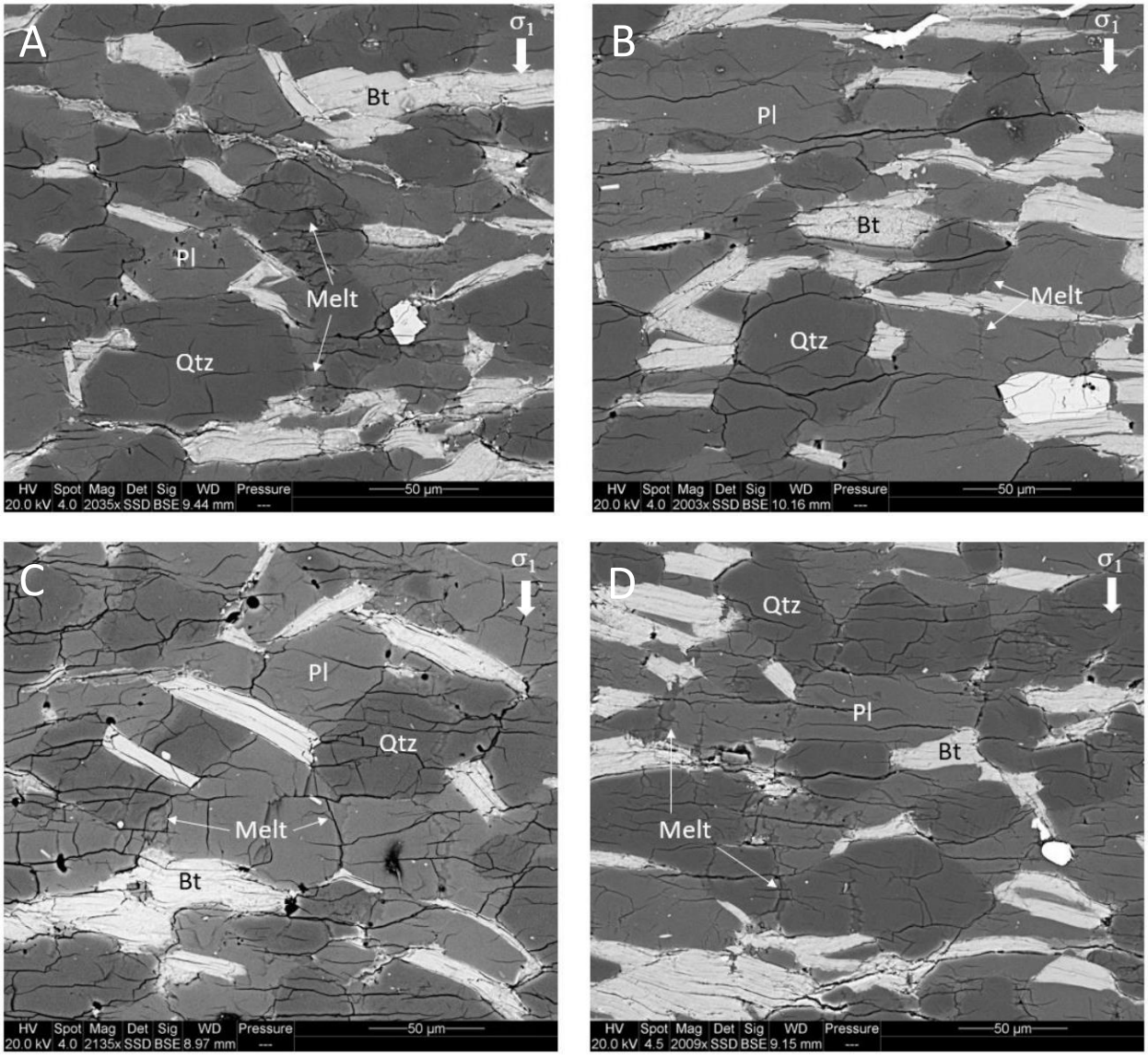

Figure 14. Melt pockets and single grain channels along grain boundaries, as well as cutting through grains observed in Gneiss Minuti F90-L90 cores (A and B). Similar topology was seen in the Gneiss Minuti F45-L45 core from GM_004 (C) and F45-L90 core from GM_016 (D).

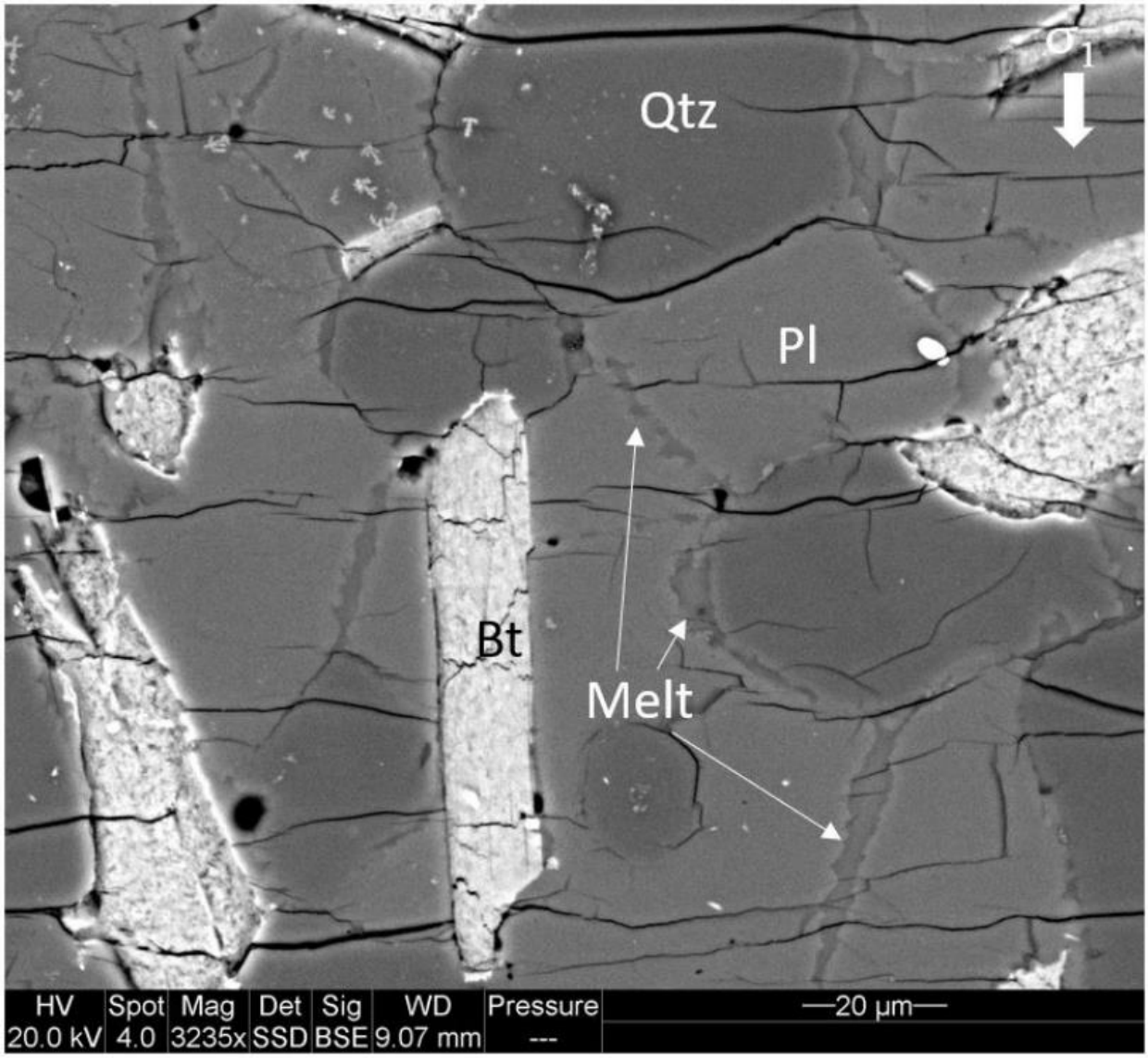

Figure 15. Interconnected vertical melt channels spanning multiple grains in the F0-L0 core from the Gneiss Minuti sample GM_005.

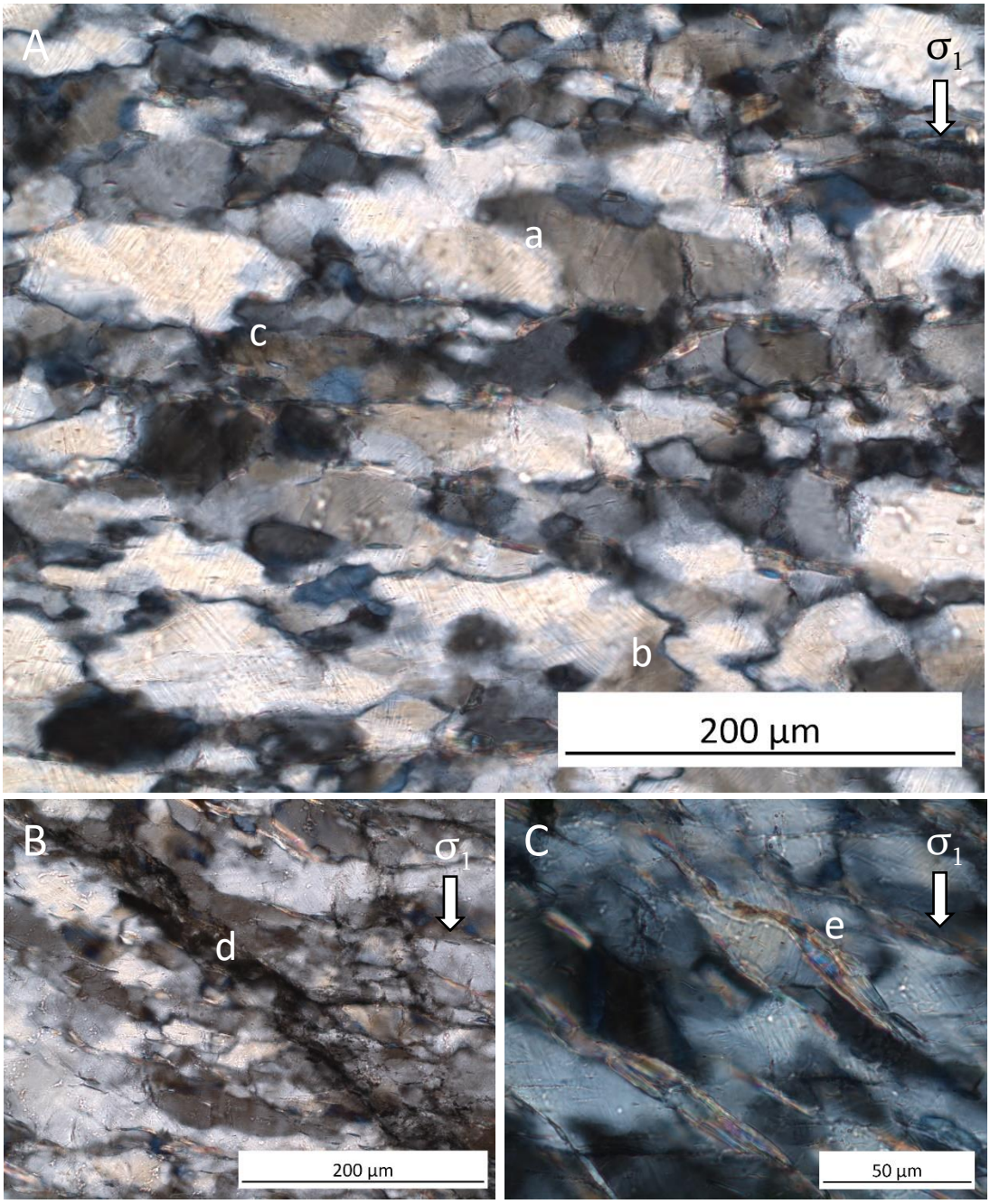

Figure 16. Optical images of deformed Moine Thrust quartzite showing undulatory extinction (a), deformation lamellae (b), and grain boundary bulging (c) in the quartz in the orientation F90-L90 sample. Localization (d) was also observed along muscovite rich beds in the F45-L45 sample. The muscovite grains also sometimes showed kinks or were sheared (e). (Experiment information: F90-L90 and F45-L45, T = 900°C)

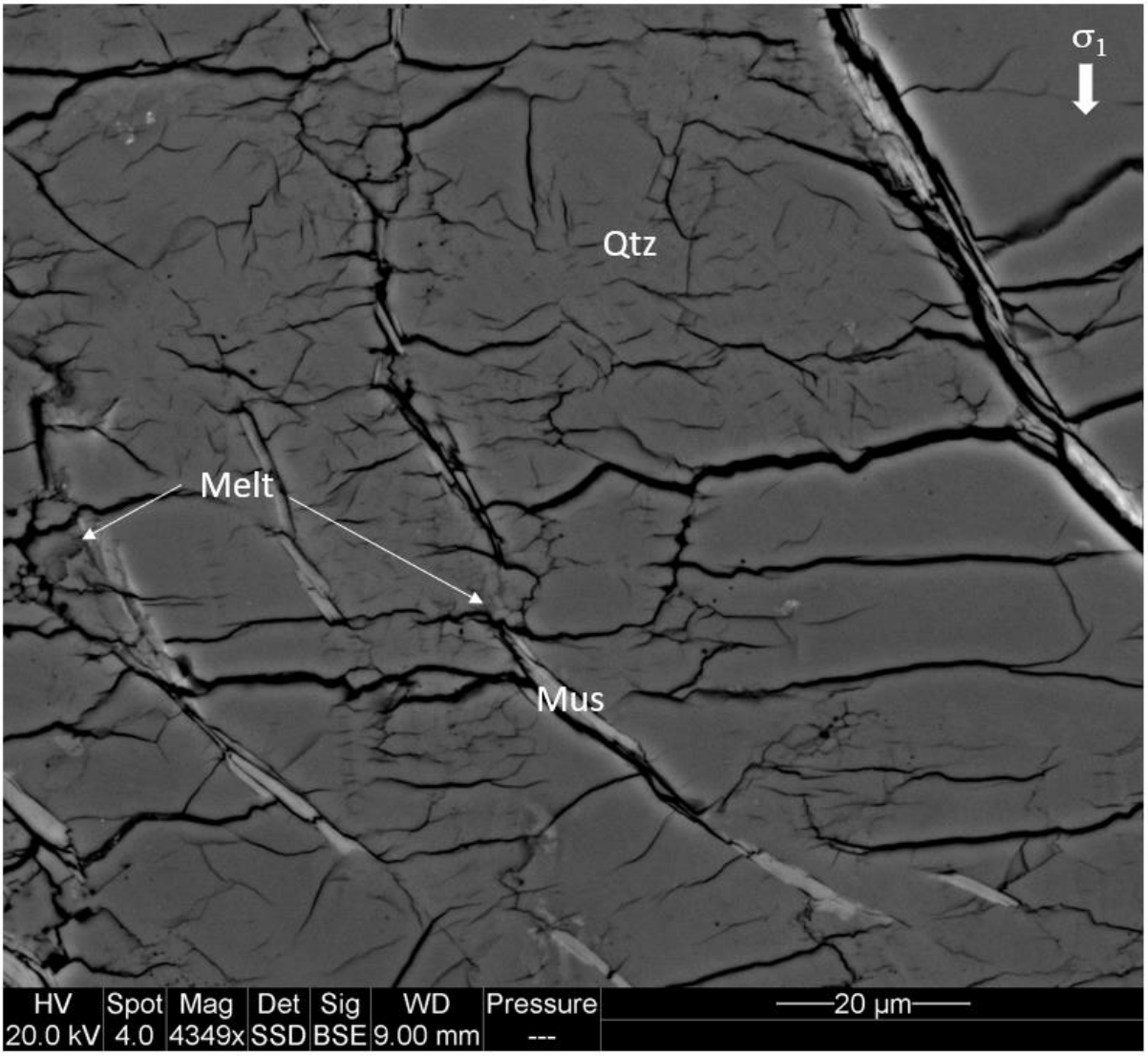

Figure 17. Small, scattered melt pockets observed in the F0-L0 orientation from the Moine Thrust quartzite sample GM_022. The foliation buckled during deformation and is no longer parallel to the compression direction.

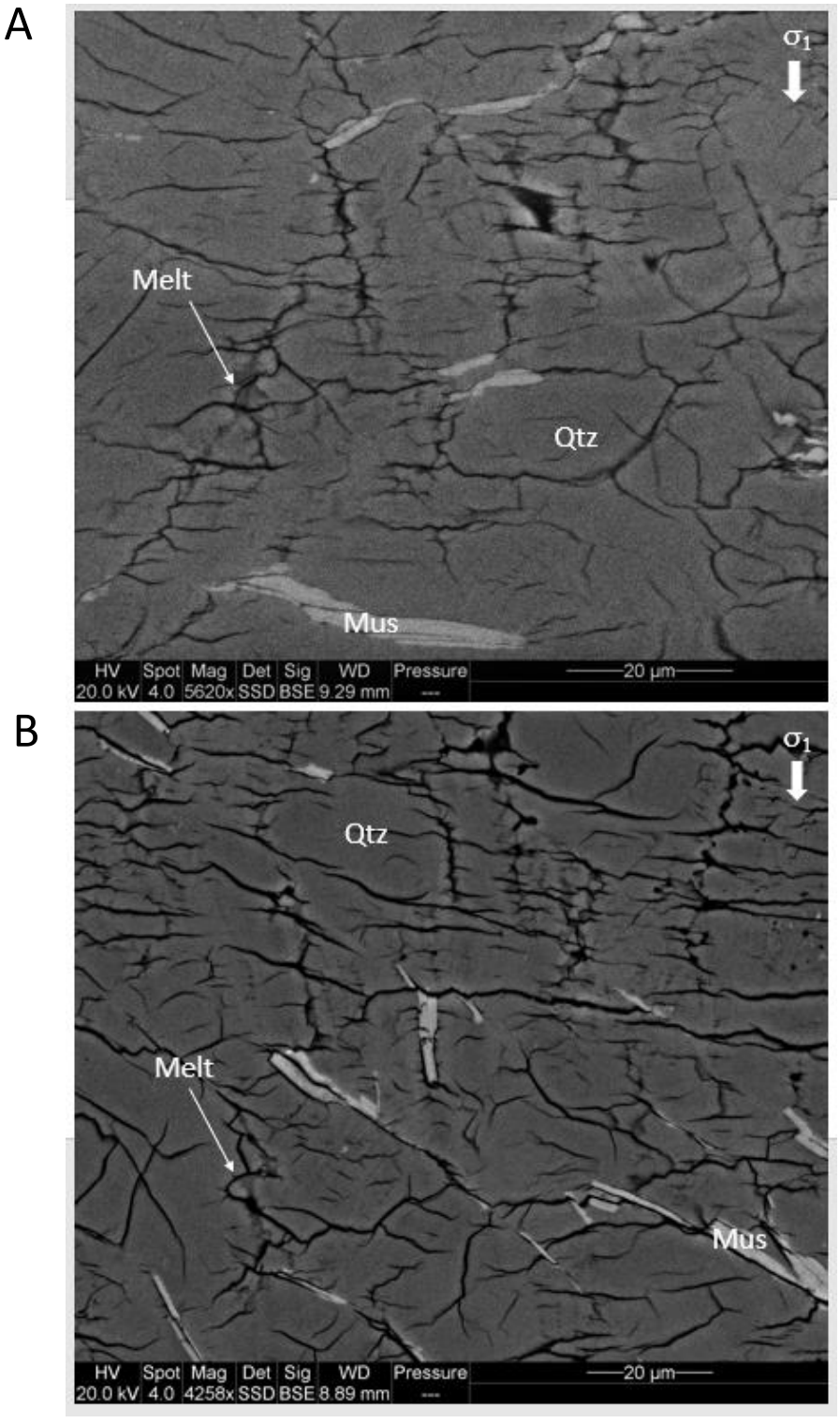

Figure 18. Small, vertical melt channels cutting through quartz grains and across the foliation in the Moine Thrust quartzite with foliation in the F90-L90 orientation (A) and in the F45-L90 orientation (B).

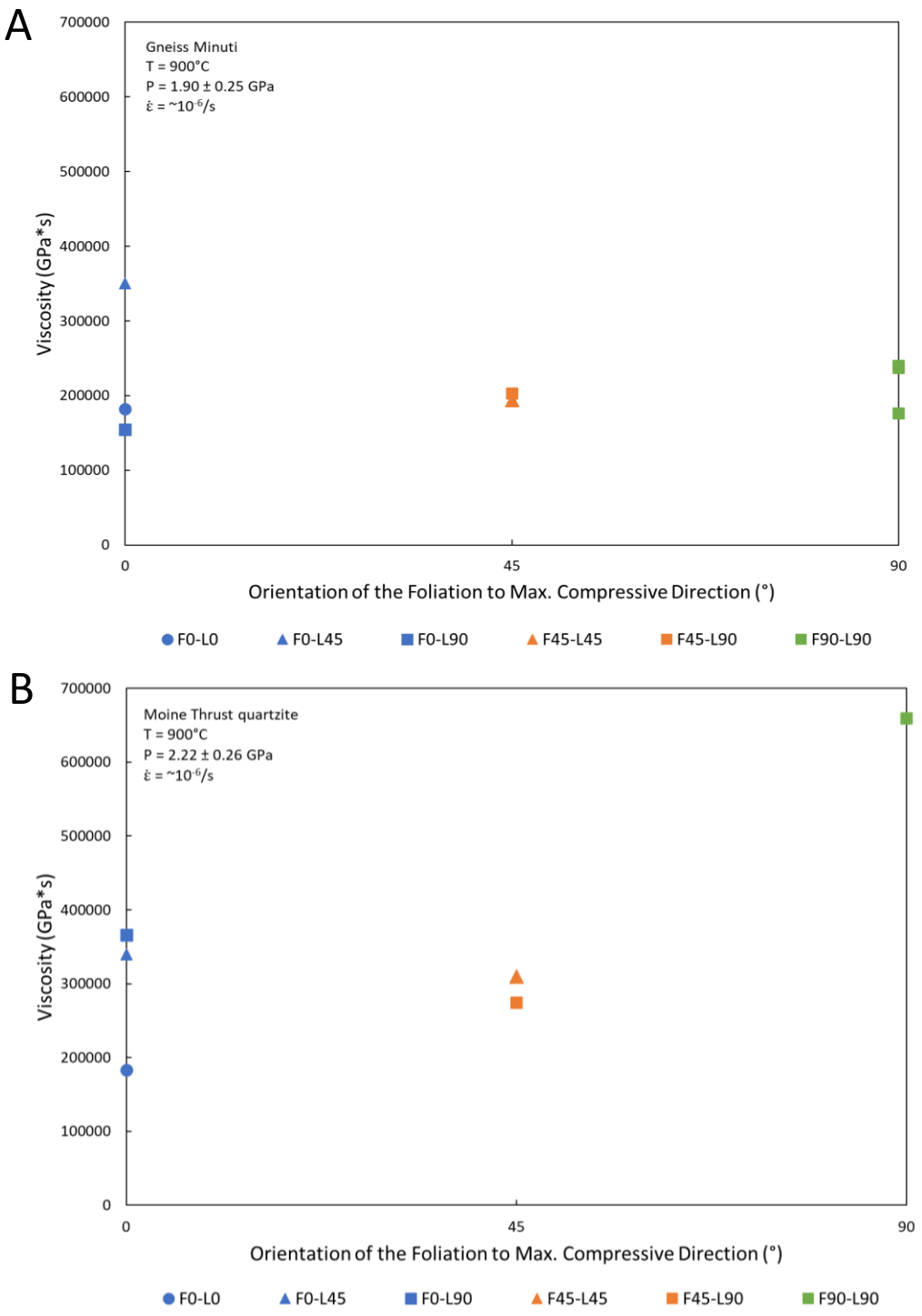

Figure 19. The viscosity of the cores in all the orientations to the foliation and lineation of the Gneiss Minuti (A) and Moine Thrust quartzite (B). The Moine Thrust quartzite samples show a larger range of viscosities than the Gneiss Minuti samples.

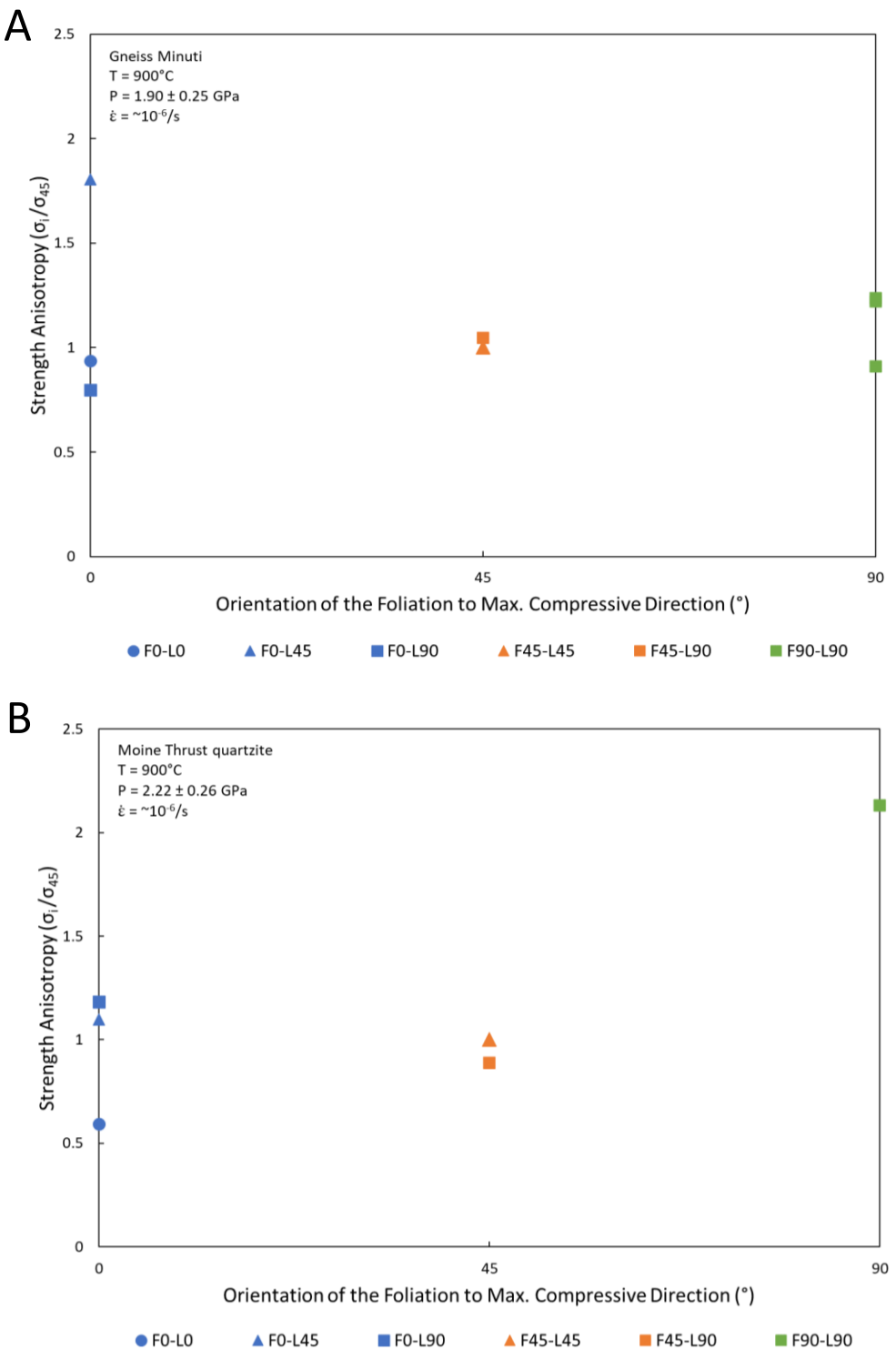

Figure 20. The strength anisotropy between the Gneiss Minuti samples (A) and Moine Thrust quartzite samples (B).

Appendix A. Assembly Procedure

Materials

- 1 fired pyrophyllite cube
- 1 graphite furnace in Al sleeve
- 1 boron nitride sleeve
- 2 regular Al pistons
- 1 1.5 mm diameter platinum cylinder 3.0 to 3.2 mm in height and 4.8 to 5.0 mm in length
- 2 platinum disks 1.8 mm in diameter
- 2 platinum disks 1.5 mm in diameter
- 4 rhenium squares/rectangles 1 to 1.5mm across
- Powered garnet or small Al piston
- 2 rock cores that are 1.5 mm in diameter and 1.2-1.3 mm in length

Material Prep

- The pyrophyllite cube, graphite furnace in Al sleeve, boron nitride sleeve, and the Al pistons are used as they are.
- Grind the 1.5 mm diameter cores until they are between 1.2-1.3 mm in length using a file and clasp. Be careful and make sure the top and bottom of the cores are parallel to each other. WRITE DOWN THE FINAL LENGTH OF THE CORES.
- Use calibrator and metal cutting scissors to make the rhenium squares/rectangles. Be careful with cutting them; they will fly and get lost. Before putting the rhenium into the assembly flatten the pieces.
- Use the 1.5 mm hole punch to make the 1.5 mm platinum disks. A scalpel and 1.5 mm rod can be used to make the disks as circular as possible. This can be done by placing the rod on the disk and using the scalpel to cut off any excess material.
- The platinum cylinder can be made by using the calibrator to measure the lengths and fine scissors to cut the metal into a rectangle. Once the rectangle is cut, use your thumb and index finger to roll the rectangle around the 1.5 mm rod to make a cylinder 1.5 mm in diameter.

Assembly Order

- Put the graphite furnace in Al sleeve into the fired pyrophyllite cube. Use a rod to push one of the Al regular pistons into this assembly (cube + furnace in Al sleeve) so that it is snug at one end. Place a small slither of tape on the end with the piston to assure nothing falls out during the assembly construction process.
- Now looking down into the assembly, place a 1.8 mm platinum disk into the assembly so that it sits on the inside surface of the Al piston. Next, place the boron nitride sleeve into the assembly on top of the platinum disk. When looking into the assembly again, you should only see platinum at the bottom of the boron nitride sleeve.
- Place the platinum cylinder into the boron nitride sleeve, which can be done with tweezers. Make sure the cylinder does not stick up too much over the boron nitride sleeve or not enough.
- Place a rhenium disk inside the platinum cylinder so that it is lying flat on the exposed platinum and so that the longest axis aligns with one of the diagonals of the cube. After this placement has been done, mark the diagonal on the cube with a sharpy perpendicular to the longest axis of the rhenium piece. This line will signal the beamline direction.
- Place a 1.5 mm platinum disk into the assembly next.
- After the platinum disk, you will now put in your first core. The core should be placed into the assembly so that the strike of the foliation is parallel to the beamline you marked. After determining the proper placement of the core, it can carefully be put into the assembly by wetting the end of the 1.5 mm rod. The water tension can be used to put the core into the assembly without significantly moving it from its desired orientation.
- Follow the core with another rhenium piece (try to get the longest axis perpendicular to the beamline) and then put in a 1.5 mm platinum disk.
- Next, you will either need to fill the assembly with crushed garnet powder or one of the small Al pistons depending on the discretion of Dr. Holyoke.
    - Garnet: subtract the length of your two cores from 1.3 mm. The number you get will be the depth of garnet powder you need within the cylinder. Scoop the garnet into the assembly, making sure to compress it tightly. The depth of the garnet can

be checked by marking the length of the second core (the one not in the assembly) on the end of a rob and filling the assembly until you can see this mark.

    - Small Al piston: subtract the length your two cores from 1.3 mm. The number you get is the length of the small Al piston you need. Use a filer and clasp to file the piston down to the desired length and place in the assembly.
- Place a 1.5 mm platinum disk on top of the compressed garnet powder/small Al piston. Next put in a rhenium piece, the second core, another rhenium piece, and then the second 1.8 mm platinum disk in the order listed. These items are put in the same ways described above keeping in mind the beamline direction. The 1.8 mm platinum disk should be sitting at the top of the boron nitride sleeve/platinum cylinder.
- Top off the assembly with the second regular Al piston. Make sure it is secure in the assembly and does not stick up too far.

Helpful Tips

- Use tweezers with the bend ends to place the metals into the assembly.
- If the small Al piston is too small to put in the clasp, use your finger to shorten it against the file.
- Take a break if you start getting frustrated.
- Do not grind the rock cores too fast; it will cause rough ends.

Appendix B. Summary of the Gneiss Minuti phase data from each experiment.

Sample	Material	Foliation/Lineation Orientation	Phase	Area (µm)	Diameter (µm)	Major Length (µm)	Minor Length (µm)	Aspect Ratio	Orientation Angle (°)
GM_004	Gneiss Minuti	F45-L45	Biotite	687.01	26.91	52.18	14.78	3.53	130.28
			Quartz	1246.09	36.64	48.27	28.30	1.71	93.39
			Plagioclase	1164.04	35.36	48.96	26.30	1.86	119.04
			Melt	54.01	6.47	10.91	4.11	2.65	84.44
		F90-L90	Biotite	588.62	25.47	49.89	13.82	3.61	85.81
			Quartz	1258.25	37.53	49.80	29.01	1.72	92.63
			Plagioclase	1035.71	33.57	49.43	23.46	2.11	80.82
			Melt	57.57	7.06	12.93	4.18	3.10	65.28
GM_005	Gneiss Minuti	F0-L0	Biotite	673.48	27.59	44.05	18.30	2.41	81.79
			Quartz	1429.97	39.84	48.81	32.85	1.49	87.54
			Plagioclase	1438.57	39.45	52.50	30.31	1.73	80.93
			Melt	59.62	7.17	11.78	4.68	2.52	86.12
		F90-L90	Biotite	516.95	23.90	44.42	13.57	3.27	95.14
			Quartz	1342.69	38.16	51.06	29.02	1.76	109.33
			Plagioclase	1059.91	34.57	50.34	24.59	2.05	82.36
			Melt	43.01	5.59	9.01	3.59	2.51	99.46
GM_016	Gneiss Minuti	F45-L90	Biotite	412.95	21.36	42.17	11.43	3.69	96.45
			Quartz	1040.72	33.50	43.44	26.23	1.66	104.64
			Plagioclase	839.09	30.59	42.24	22.57	1.87	112.86
			Melt	33.86	5.90	10.06	3.69	2.72	93.79
		F90-L90	Biotite	940.84	32.04	60.98	17.72	3.44	113.11
			Quartz	1190.54	35.83	47.70	27.56	1.73	107.57
			Plagioclase	1232.67	37.41	52.63	27.68	1.90	116.67
			Melt	23.00	4.55	8.27	2.66	3.11	78.63
GM_017	Gneiss Minuti	F0-L45	Biotite	626.42	24.81	41.71	15.30	2.73	90.10
			Quartz	1390.69	38.84	47.59	32.37	1.47	83.28
			Plagioclase	1323.10	36.38	47.60	28.39	1.68	96.56
			Melt	27.03	5.12	10.41	2.80	3.72	85.33
		F0-L90	Biotite	465.60	21.94	36.30	13.87	2.62	93.63
			Quartz	1203.32	34.75	43.57	28.17	1.55	87.51
			Plagioclase	993.76	32.63	41.65	26.01	1.60	91.86
			Melt	20.53	4.47	8.08	2.67	3.03	83.53